Myocardial-specific ablation of *Jumonji and AT-rich interaction domain–containing 2* (*Jarid2*) leads to dilated cardiomyopathy in mice

Received for publication, August 30, 2018, and in revised form, January 18, 2019 Published, Papers in Press, January 30, 2019, DOI 10.1074/jbc.RA118.005634

Eunjin Cho[‡§], **HyunJun Kang**[¶], **Dae-Ki Kang**[‖], **and Youngsook Lee**[‡§1]

From the [‡]*Department of Cell and Regenerative Biology, the* [§]*Molecular and Cellular Pharmacology Graduate Program, and the* [¶]*National Primate Research Center, University of Wisconsin-Madison, Madison, Wisconsin 53705 and the* [‖]*Department of Computer Engineering, Dongseo University, Busan 47011, South Korea*

Edited by Qi-Qun Tang

Cardiomyopathy is a common myocardial disease that can lead to sudden death. However, molecular mechanisms underlying cardiomyopathy remain unclear. Jumonji and AT-rich interaction domain–containing 2 (Jarid2) is necessary for embryonic heart development, but functions of Jarid2 after birth remain to be elucidated. Here, we report that myocardial-specific deletion of *Jarid2* using *αMHC*::*Cre* mice (*Jarid2*$^{\alpha MHC}$) causes dilated cardiomyopathy (DCM) and premature death 6–9 months after birth. To determine functions of Jarid2 in the adult heart and DCM, we analyzed gene expression in the heart at postnatal day (p)10 (neonatal) and 7 months (DCM). Pathway analyses revealed that dysregulated genes in *Jarid2*$^{\alpha MHC}$ hearts at p10, prior to cardiomyopathy, represented heart development and muscle contraction pathways. At 7 months, down-regulated genes in *Jarid2*$^{\alpha MHC}$ hearts were enriched in metabolic process and ion channel activity pathways and up-regulated genes in extracellular matrix components. In normal hearts, expression levels of contractile genes were increased from p10 to 7 months but were not sufficiently increased in *Jarid2*$^{\alpha MHC}$ hearts. Moreover, Jarid2 was also necessary to repress fetal contractile genes such as *TroponinI1, slow skeletal type* (*Tnni1*) and *Actin alpha 2, smooth muscle* (*Acta2*) in neonatal stages through ErbB2-receptor tyrosine kinase 4 (ErbB4) signaling. Interestingly, *Ankyrin repeat domain 1* (*Ankrd1*) and *Neuregulin 1* (*Nrg1*), whose expression levels are known to be increased in the failing heart, were already elevated in *Jarid2*$^{\alpha MHC}$ hearts within 1 month of birth. Thus, we demonstrate that ablation of *Jarid2* in cardiomyocytes results in DCM and suggest that Jarid2 plays important roles in cardiomyocyte maturation during neonatal stages.

Heart failure is a major cause of mortality affecting 40 million people globally (1). Prolonged exposure to pathological and physiological stresses in the adult myocardium triggers adaptive responses followed by maladaptive responses, including the disruption of transcriptional homeostasis and re-expression of fetal sarcomere and metabolism genes. Persistent volume overload induces axial cardiomyocyte lengthening and chamber dilation, known as eccentric remodeling or dilated cardiomyopathy (DCM),[2] resulting in reduced systolic function (2). In contrast, pressure overload induces radial cardiomyocyte widening and ventricular wall thickening, resulting in concentric growth or hypertrophic cardiomyopathy (HCM) with diastolic dysfunction (3). DCM and HCM are the most common forms of cardiomyopathy that can lead to sudden death (4). Many mutations in sarcomere genes, such as *Myosin heavy chain 7* (*Myh7*, βMHC), *Tropomyosin 1* (*Tpm1*), and *Cardiac troponin T* (*Tnnt2*) cause both DCM and HCM. However, molecular and genetic causes of DCM are more heterogenous than HCM (5–7), which include cytoskeletal, costamere, and nuclear membrane proteins (8, 9). Thus, the molecular mechanisms underlying DCM are not fully understood.

Cardiomyocytes undergo dramatic molecular and developmental changes during the first 2 weeks after birth (herein, referred to as "neonatal" stages), to generate mature functioning cardiomyocytes (10, 11). These changes include the regulation of gene expression and isoform switching from fetal to adult forms, which are involved in contractility, calcium handling, energy utilization, and cell proliferation. In the mouse ventricle, βMHC, the predominant isoform during fetal stages, is replaced by αMHC after birth (10). Expression of metabolic genes for glycolytic processes is decreased, whereas oxidative and fatty acid metabolism genes are induced in the postnatal

This work was supported in part by National Institutes of Health Grant HL067050 and American Heart Association Grant 12GRNT12070021 (to Y. L.). The authors declare that they have no conflicts of interest with the contents of this article. The content is solely the responsibility of the authors and does not necessarily represent the official views of the National Institutes of Health.

This article contains Tables S1–S4, Figs. S1–S3, and supporting data.

The data discussed in this publication have been deposited in NCBI's Gene Expression Omnibus and are accessible through GEO Series accession number GSE118945.

[1] To whom correspondence should be addressed: Dept. of Cell and Regenerative Biology, School of Medicine and Public Health, University of Wisconsin-Madison, Wisconsin Institutes for Medical Research II, 1111 Highland Avenue, Madison, WI 53705; Tel.: 608-265-6352; Fax: 608-262-7306; E-mail: youngsooklee@wisc.edu.

[2] The abbreviations used are: DCM, dilated cardiomyopathy; Jarid2, Jumonji A/T-rich interaction domain-2; *Jarid2*$^{\alpha MHC}$, *αMHC*::*Cre/+; Jarid2f/f* genotype; PPDE, posterior probability of differential expression; DE, differentially expressed; p*n*, postnatal day *n*; HCM, hypertrophic cardiomyopathy; Nrg, neuregulin; KO, knockout; qRT-PCR, quantitative real-time PCR; X-gal, 5-bromo-4-chloro-3-indolyl β-D-galactoside; H&E, hematoxylin and eosin; CSA, cross-sectional area; WGA, wheat germ agglutinin; LV, left ventricle/ventricular; LVID;d, LV inner diameter at end diastole; LVID;s, LV inner diameter at end systole; EF, ejection fraction; FS, fractional shortening; GO, Gene Ontology; BP, biological process; CC, cellular component; SERCA, sarcoplasmic/endoplasmic reticulum Ca^{2+}-ATPase; MF, molecular function; PPAR, peroxisome proliferator–activated receptor; TPM, transcript per million; FDR, false discovery rate.

heart. Mitochondrial density increases as the metabolic rate increases (12). Cardiomyocyte proliferation in mice ceases during the neonatal period, and physiological hypertrophic growth occurs (13). However, it is poorly understood how these transitions are integrated during neonatal stages and how alterations in these changes contribute to heart failure later in life. Neuregulins (Nrgs) are secreted from the endocardium/endothelial cells and bind to ErbB2 and ErbB4 receptors in cardiomyocytes (14). Nrg1–ErbB signaling has crucial roles in cardiac development and function (15) and activate Akt, Erk, or Jnk pathways required for cell growth and survival (16). Nrg1 improves heart function (16), but this is controversial (17, 18). Thus, it is unclear how Nrg1–ErbB signaling is regulated and what their roles are in the progression of heart failure.

Jarid2 is required for normal embryonic development. Knockout (KO) of *Jarid2* in mice causes developmental defects in the heart, liver, or hematopoietic tissues and lethality (19). Endothelial/endocardial deletion of *Jarid2* shows cardiac defects recapitulating those in *Jarid2* KO mice (20). Early deletion of *Jarid2* in the cardiac progenitors using *Nkx2.5*::*Cre* mice leads to cardiac morphological defects and death within 1 day after birth, but *Jarid2* deletion in the differentiated myocardium does not exhibit developmental abnormalities (21). Jarid2 functions as an epigenetic regulator by interacting with methyltransferase enzymes (22). Jarid2 is a component of Polycomb repressive complex 2, a histone H3 lysine 27 (H3K27) methyltransferase. We have demonstrated that Jarid2 and polycomb repressive complex 2 accumulate on the *Isl1* promoter during heart development and repress *Isl1* expression (21). Jarid2 recruits Setdb1 on the *Notch1* promoter and represses *Notch1* expression via H3K9 methylation in endothelial/endocardial cells of the developing heart (23). Jarid2 can repress transcriptional activity of cardiac transcription factors (24). Interestingly, JARID2 expression is reduced in heart failure patients (25). In mice, reduced Jarid2 expression is associated with cardiac hypertrophy (26), implying potential roles of Jarid2 in the adult heart. However, roles of Jarid2 in the adult heart remains unclear.

Here, we analyzed mice with a cardiomyocyte-specific deletion of Jarid2 using *αMHC*::*Cre* mice. All *Jarid2*$^{\alpha MHC}$ mice died by 9 months of age with DCM. Gene expression profiling was performed on p10 and 7-month hearts during neonatal stages and DCM, respectively. Our pathway analyses of the neonatal heart from *Jarid2*$^{\alpha MHC}$ mice indicated that heart development and muscle contraction pathways were significantly dysregulated, despite normal heart morphology at this age. Specifically, immature sarcomere genes, such as *Troponin I type 1* (*Tnni1*) and *Smooth muscle alpha-actin 2* (*Acta2*), and heart failure–associated genes were up-regulated in *Jarid2*$^{\alpha MHC}$ hearts at p10. At 7 months, *Jarid2*$^{\alpha MHC}$ hearts were enriched with dysregulated genes in collagen fibril organization and metabolic process pathways. Further, a subset of sarcomeric genes were increased from p10 to 7 months in the normal heart such as *Cardiac alpha-actin* (*Actc1*), *Myh6*, *Tnni3*, *Tnnt2*, *Tropomyosin* (*Tpm1*), *Myosin regulatory light chain* (*Myl2*), and *Phospholamban* (*Pln*), but not in *Jarid2*$^{\alpha MHC}$ hearts. Interestingly, *Nrg1*, *ErbB4*, and *Ankyrin repeat domain 1* (*Ankyd1*) expression levels were already dysregulated in *Jarid2*$^{\alpha MHC}$ hearts prior to DCM. Thus, our data suggest that Jarid2 is required for neonatal myocardial maturation, which impacts on adult cardiac function and homeostasis.

Results

Generation of mice with cardiac-specific deletion of Jarid2

Jarid2 is indispensable for normal embryonic development (20, 21, 27). To determine cardiac-specific roles of Jarid2 in the adult heart, we analyzed *Jarid2*$^{\alpha MHC}$ mice, in which *αMHC*::*Cre* specifically inactivates the conditional *Jarid2 f/f* allele in differentiated cardiomyocytes (28, 29). PCR analyses of genomic DNAs showed that *Jarid2* was deleted only in the heart but not in the tail of *Jarid2*$^{\alpha MHC}$ mice because a *Jarid2* floxed-out band (354 bp) was detected only in the heart of *Jarid2*$^{\alpha MHC}$ but not in the control heart or in the tail (Fig. 1*A*). qRT-PCR data confirmed a reduction in *Jarid2* transcripts in *Jarid2*$^{\alpha MHC}$ *versus* control hearts at p10 (Fig. 1*B*). Given efficient deletions of *Jarid2* floxed allele by various Cre (21, 29) and increased noncardiomyocyte populations after birth, the unrecombined *Jarid2 f/f* allele in the 3-month-old heart (Fig. 1*A*) or residual mRNA (Fig. 1*B*) can be attributed to noncardiomyocytes. Immunostaining and Western blotting data also showed a marked reduction of Jarid2 levels in *Jarid2*$^{\alpha MHC}$ hearts (Fig. 1, *C* and *D*). To examine Jarid2 levels in the normal heart at different stages, we performed X-gal staining on tissue sections from heterozygous *Jarid2* gene trapped mice, in which *LacZ* expression recapitulates endogenous *Jarid2* expression (27). X-gal staining was reduced by 1 month of age (Fig. 1*E*). Western blotting confirmed that Jarid2 expression was high until p2 but significantly reduced in the adult heart (Fig. 1*F*). These data indicate that Jarid2 continues to be expressed in the neonatal heart followed by a marked decrease at approximately 1 month of age, implying an important role of Jarid2 during neonatal stages.

Jarid2$^{\alpha MHC}$ *mice exhibited dilated cardiomyopathy and premature death*

The *Jarid2*$^{\alpha MHC}$ mice showed expected Mendelian ratios and no gross morphological defects in the embryonic (20) or young adult heart (Fig. S1*A* and Table S1). However, the mutant mice exhibited 100% mortality by 9 months (Fig. 2*A*), likely because of heart failure. Thus, *Jarid2*$^{\alpha MHC}$ hearts at 7 months were subjected to histological examination. The mutant heart was enlarged compared with controls at 7 months (Fig. 2*B*). Hematoxylin and eosin (H&E) staining images showed similar ventricular wall or septal thickness in the mutant heart (Fig. 2*C*). Apoptosis levels were not significantly changed in mutant hearts *versus* controls (Fig. S1*B*). The cross-sectional area (CSA) of cardiomyocytes was measured by wheat germ agglutinin (WGA) staining to demarcate plasma membrane boundaries in the ventricular myocardium (Fig. 2*D*). *Jarid2*$^{\alpha MHC}$ hearts did not show any significant changes in CSA (Fig. 2*F*) and a total number of cells in the same square area (Fig. S1*C*). Increased fibrosis was detected in mutant *versus* control hearts as indicated by PicroSirius red staining (Fig. 2*E*). Expression of heart failure markers, *Nppa*, *Nppb*, *Myh7*, and *Acta1* were normal at 3 months in *Jarid2*$^{\alpha MHC}$ hearts but significantly

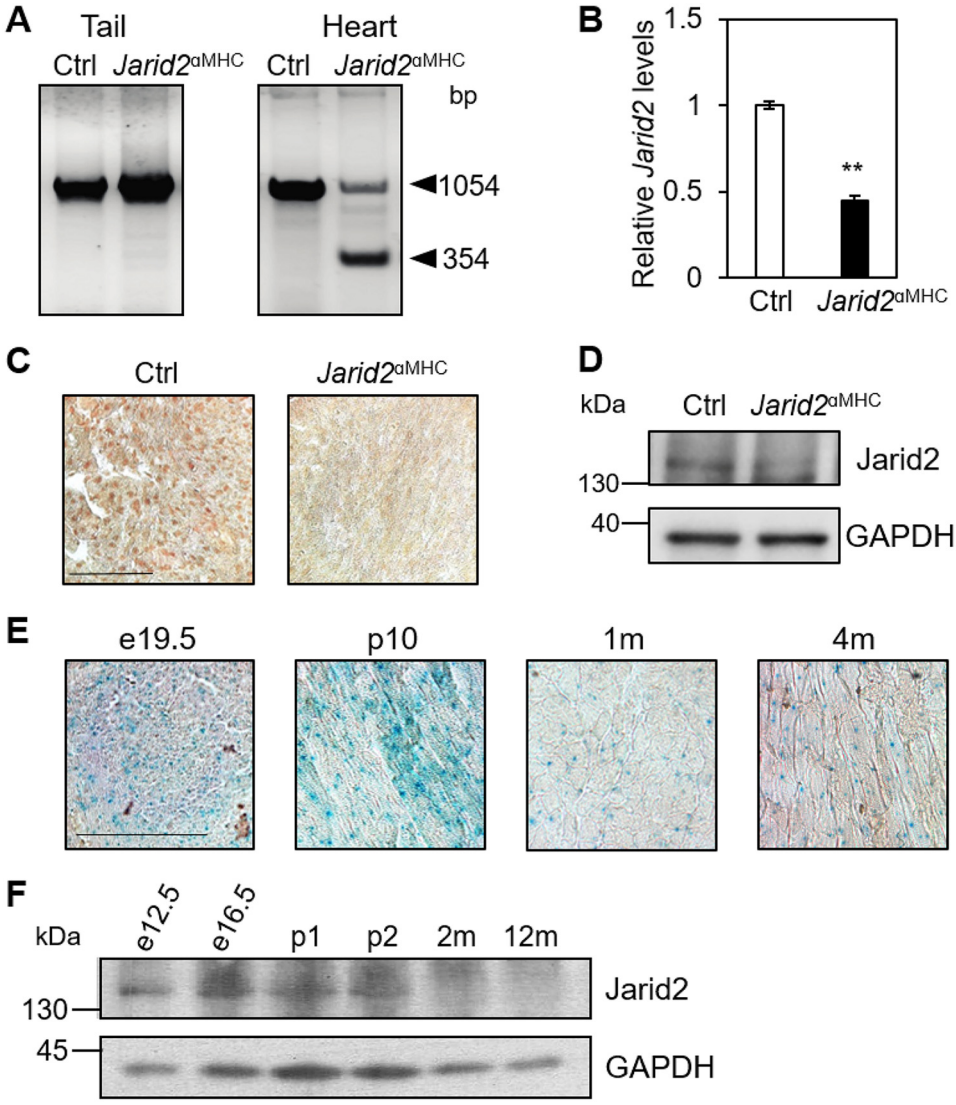

Figure 1. Conditional deletion of Jarid2 and age-dependent expression levels of Jarid2. *A*, genomic DNAs were isolated from the tail and the heart at 3 months, and PCR was performed with primers detecting floxed *Jarid2* (1054 bp) or floxed out *Jarid2* (354 bp) band. *B*, qRT-PCR was performed on p10 hearts to determine *Jarid2* expression levels. The expression levels were normalized to control (*Ctrl*) levels ($n = 3$). *C*, immunostaining was performed on p10 hearts with Jarid2 antibody (*brown*). *Scale bar*, 100 μm. *D*, Jarid2 protein levels were detected by Western blotting on p10 hearts. The GAPDH was used as a loading control. *E*, LacZ staining was performed on the frozen sections of *Jarid2* heterozygous hearts (27) at different stages. *Scale bar*, 100 μm. *F*, Jarid2 protein levels of WT hearts were detected by Western blotting on embryonic (*e*) and postnatal hearts. The GAPDH was used as a loading control. *m*, month(s).

increased at 7 months compared with controls (Fig. 2*G*). These data suggest that *Jarid2*$^{\alpha MHC}$ mice do not exhibit cardiomyopathy at 3 months but progress to cardiomyopathy, leading to premature death between 6 and 9 months of age.

Next, we investigated cardiac structural and functional parameters by echocardiography at 3 and 7 months of age (Table 1). *Jarid2*$^{\alpha MHC}$ mice at 7 months showed increases in left ventricular inner diameter at end diastole (LVID;d) and end systole (LVID;s) and LV mass/body weight ratios as compared with controls (Fig. 3, *A–C*). The dilation was not accompanied by an alternation in interventricular septal or posterior wall thickness, whereas LV volumes were significantly increased at end diastole and end systole, indicating the enlarged and dilated LV (Table 1). The left ventricular thickness/radius ratio (LV wall thickness/chamber radius) was significantly reduced in *Jarid2*$^{\alpha MHC}$ *versus* control hearts, indicating ventricular dilation. Decreases in ejection fraction (EF; Fig. 3*D*) and the percentages of fractional shortening (FS; Fig. 3*E*) were detected at 7 months, indicating defective cardiac contractility and DCM.

To determine the time-dependent changes in cardiac parameters of *Jarid2*$^{\alpha MHC}$ mice, echocardiography was performed at 3 months (Table 1). Interestingly, *Jarid2*$^{\alpha MHC}$ mice showed hyperperforming hearts as evidenced by increases in stroke volume, EF, FS, and cardiac output (Fig. 3, *D–F*). However, LV chamber dimensions remained similar to controls. Histological analyses of *Jarid2*$^{\alpha MHC}$ hearts at 3 months did not show morphological defects (Fig. S2). Thus far, our data indicate that *Jarid2*$^{\alpha MHC}$ mice exhibit hyperperforming compensating hearts at 3 months followed by decompensation and pathological remodeling by 6–7 months of age. Aortic peak velocity in the mutant heart was not changed compared with the control.

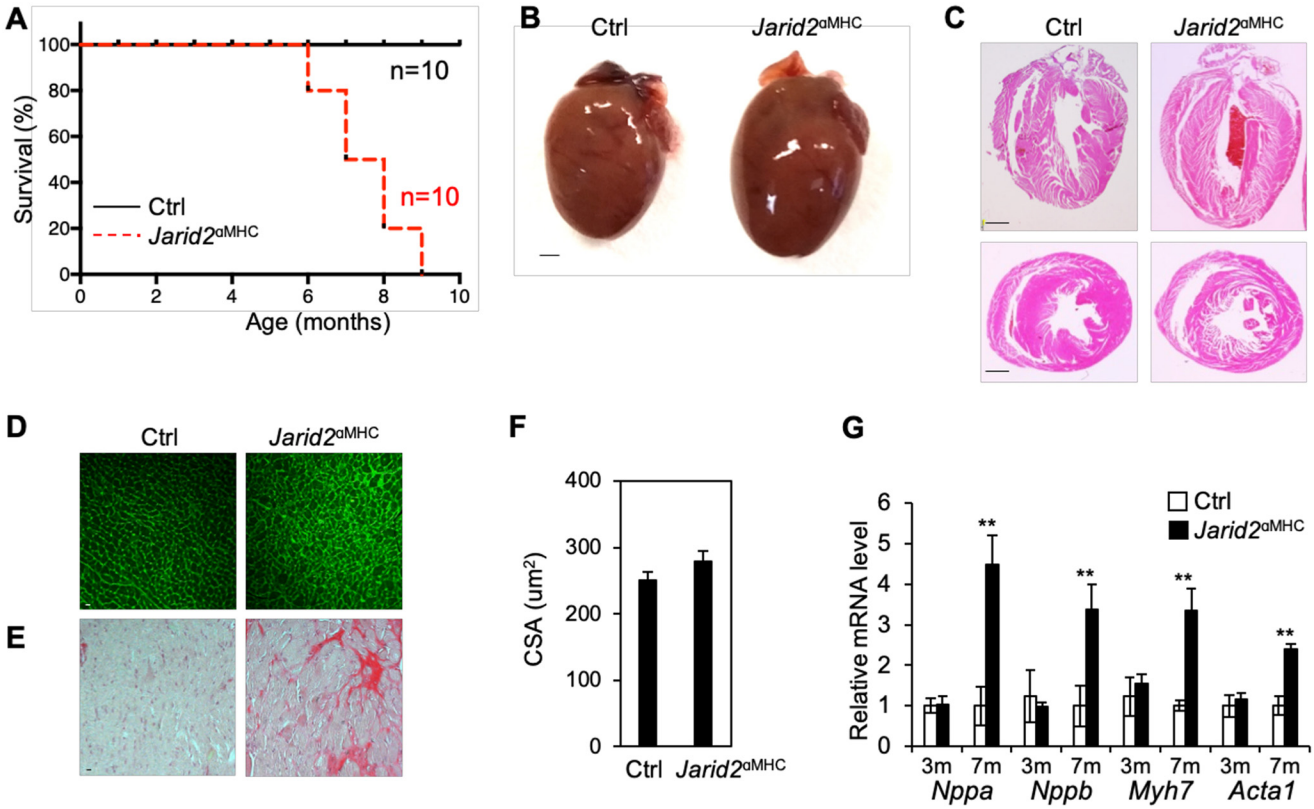

Figure 2. *Jarid2*$^{\alpha MHC}$ mice died at 6–9 months of age. *A*, Kaplan–Meier survival curves of control (*Ctrl*) and *Jarid2*$^{\alpha MHC}$ mice were assessed by log-rank test. $p < 0.001$ ($n = 10$). *B*, gross morphology of *Jarid2*$^{\alpha MHC}$ hearts at 7 months. *Scale bar*, 1 mm. *C–E*, the frontal (*top panels*) or transverse midline (*bottom panels*) heart sections were stained with H&E (*C*), and frontal sections for WGA (*D*), or PicroSirius red (*E*) staining on control and *Jarid2*$^{\alpha MHC}$ hearts at 7 months. *Scale bar*, 1 mm. *F*, cardiomyocyte surface CSA in the left ventricular wall of 7-month hearts was measured by WGA staining using ImageJ software ($n = 3$). *G*, expression levels of hypertrophy marker genes were measured by qRT-PCR on control and *Jarid2*$^{\alpha MHC}$ hearts at 3 or 7 months and normalized to control levels ($n = 3$–5). *m*, month(s).

Table 1

Echocardiographic assessment of cardiac structure and function in *Jarid2*$^{\alpha MHC}$ mice

Evaluation of cardiac structural and functional parameters by echocardiography in *Jarid2*$^{\alpha MHC}$ and control mice at 3 and 7 months. The values are means ± S.E. PW, posterior wall; AW, anterior wall; H/R, left ventricular thickness/radius; EF, ejection fraction; FS, fractional shortening; IVRT, isovolumic relaxation time; MV E/A, the ratio of peak velocity of early to late filing of mitral inflow; BW, body weight.

	3 months		7 months	
	Control	*Jarid2*$^{\alpha MHC}$	Control	*Jarid2*$^{\alpha MHC}$
n	9	10	9	9
LVID;d (mm)	4.12 ± 0.1	4.34 ± 0.1	4.23 ± 0.1	5.22 ± 0.3[a]
LVID;s (mm)	3.33 ± 0.1	3.20 ± 0.2	3.02 ± 0.09	4.36 ± 0.37[a]
LV PW, d (mm)	0.60 ± 0.03	0.65 ± 0.02	0.67 ± 0.02	0.64 ± 0.02
LV PW, s (mm)	0.77 ± 0.03	0.90 ± 0.03[a]	0.78 ± 0.02	0.77 ± 0.02
LV AW, d (mm)	0.60 ± 0.03	0.66 ± 0.02	0.67 ± 0.02	0.64 ± 0.02
LV AW, s (mm)	0.82 ± 0.04	0.89 ± 0.03	0.77 ± 0.02	0.76 ± 0.02
H/R	0.29 ± 0.01	0.30 ± 0.01	0.32 ± 0.01	0.25 ± 0.01[a]
LV volume, d (μl)	79.04 ± 4.5	86.39 ± 6.9	80.83 ± 5.2	135.34 ± 19.1[a]
LV volume, s (μl)	45.54 ± 3.6	42.49 ± 5.5	35.96 ± 2.6	93.06 ± 20.8[b]
Stroke volume (μl)	33.50 ± 1.9	43.90 ± 2.3[a]	44.87 ± 3.1	42.28 ± 3.7
EF (%)	42.71 ± 2.1	51.95 ± 2.7[b]	55.37 ± 1.5	35.21 ± 4.3[a]
FS (%)	20.87 ± 1.1	26.64 ± 1.7[a]	28.65 ± 1.0	17.25 ± 2.3[a]
Heart rate (bpm)	424.44 ± 6.3	419.20 ± 11.9	485.67 ± 13.1	448.11 ± 18.1
Cardiac output (ml/m)	14.17 ± 0.7	18.47 ± 1.2[a]	21.75 ± 1.5	19.10 ± 2.0
IVRT (ms)	23.75 ± 1.5	18.46 ± 1.1[a]	19.52 ± 1.7	22.22 ± 1.7
MV E/A	1.65 ± 0.1	1.32 ± 0.1[b]	1.37 ± 0.1	1.23 ± 0.2
LV mass (mg)	90.27 ± 8.9	106.29 ± 9.7	101.87 ± 5.2	142.50 ± 14.1[b]
Body weight (g)	27.67 ± 2.0	26.70 ± 1.5	33.78 ± 1.9	33.22 ± 1.7
LV mass/BW (mg/g)	3.24 ± 0.1	3.98 ± 0.3[b]	3.06 ± 0.2	4.37 ± 0.5[b]

[a] $p < 0.01$ compared with controls.
[b] $p < 0.05$ compared with controls.

Aortic peak velocity (mm/s) values at 3 months were 1332.11 ± 120.1 and 2068.50 ± 381.4 for controls and mutants, respectively ($p = 0.10$, statistically not significant). At 7 months, it was 1817.04 ± 120.7 for controls *versus* 1497.00 ± 190.2 for mutants ($p = 0.17$, statistically not significant). Altogether, we demonstrated for the first time that Jarid2 within the myocardium is required for maintaining normal cardiac function in the adult heart.

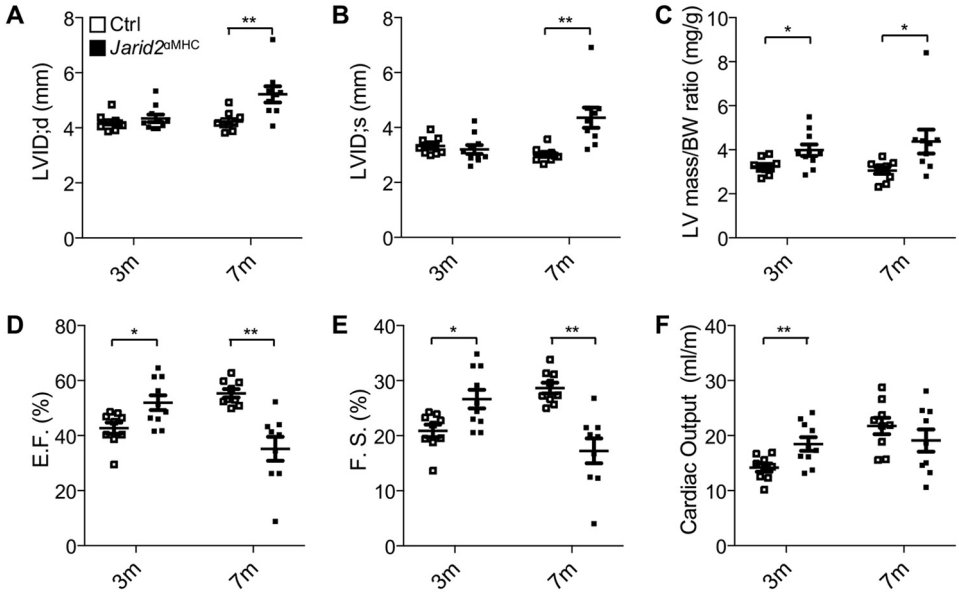

Figure 3. *Jarid2*$^{\alpha MHC}$ mice developed dilated cardiomyopathy. Cardiac structural and functional parameters were evaluated by echocardiography at 3 or 7 months of age. *Jarid2*$^{\alpha MHC}$ mice showed increased LV inner diameters at diastole (*LVID;d*, *A*) and systole (*LVID;s*, *B*) at 7 months, and LV mass to body weight ratio (*C*). Heart function was measured by ejection fraction (*EF*, *D*), fractional shortening (*F.S.*, *E*), and cardiac output (*F*). The values are means ± S.E. ($n = 9–10$). *Ctrl*, control; *m*, month(s).

Gene expression profiling in the Jarid2$^{\alpha MHC}$ *heart at neonatal stages*

The heart undergoes crucial maturation processes during the first 2 weeks after birth to achieve normal adult cardiac morphology and function (12). Jarid2 expression was significantly reduced by 1 month of age (Fig. 1, *E* and *F*), but *Jarid2*$^{\alpha MHC}$ mice did not show DCM until much later. Thus, we hypothesized that early defects during neonatal stages in the mutant heart play critical roles in the initiation and progression to DCM later in life. We set out to determine molecular changes in *Jarid2*$^{\alpha MHC}$ hearts at p10, which will provide crucial information on the function of Jarid2 in the postnatal hearts, as well as defective molecular pathways that underlie DCM pathogenesis. The *Jarid2*$^{\alpha MHC}$ heart exhibited normal morphology (Fig. 4, *A* and *B*), and hypertrophic marker genes were not altered in *Jarid2*$^{\alpha MHC}$ *versus* control hearts (Fig. 4*D*). CSA (Fig. 4*C*) and cell proliferation examined by immunostaining of Ki67 or phospho-histone H3 (Fig. S1*D*) was not altered in the *Jarid2*$^{\alpha MHC}$ heart. Together, *Jarid2*$^{\alpha MHC}$ hearts present grossly normal phenotypes at p10.

Thus, *Jarid2*$^{\alpha MHC}$ hearts at p10 would provide an excellent opportunity to investigate the molecular function of Jarid2 in the postnatal heart before the onset of secondary compensatory processes or pathological remodeling of the heart. We analyzed gene expression profiling in *Jarid2*$^{\alpha MHC}$ *versus* control hearts by performing RNA-seq at p10 (Fig. 5). We employed two different analysis methods, EBSeq (Fig. 5*A*) and DESeq2 (Fig. S3*A*), to determine differentially expressed (DE) genes between *Jarid2*$^{\alpha MHC}$ and control hearts (30). As shown in Fig. 5*B*, 61 DE genes were identified by EBSeq analysis, whereas 20 DE genes were identified by DESeq2 analysis. First, we analyzed all 72 DE genes identified by either DESeq2 or EBSeq analysis (Table S2). The majority of DE genes (54 genes, 75%) were up-regulated in the absence of *Jarid2* (Fig. 5*C* and Table S2), likely reflecting the

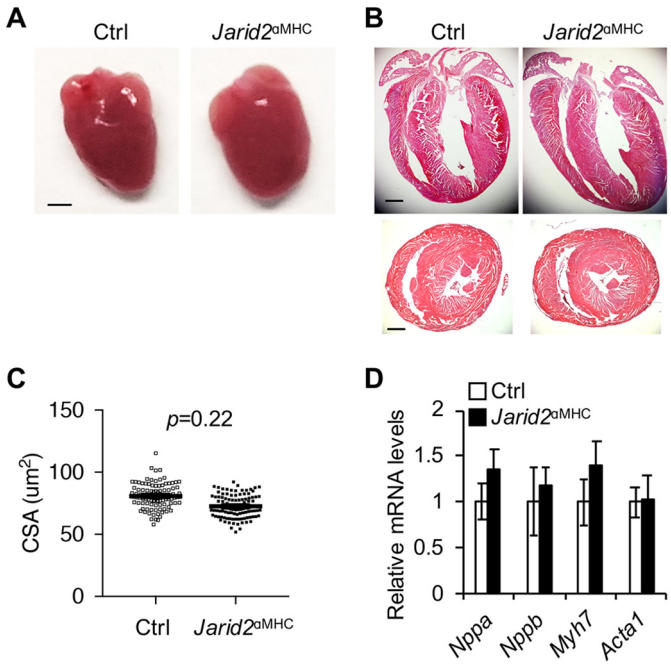

Figure 4. *Jarid2*$^{\alpha MHC}$ hearts revealed normal phenotypes at p10. *A*, whole heart images of control (*Ctrl*) and *Jarid2*$^{\alpha MHC}$ mice at p10. *Scale bar*, 1 mm. *B*, H&E staining was performed on p10 hearts on frontal (*top*) and transverse (*bottom*) sections. *Scale bar*, 500 μm. *C*, CSA was measured by WGA staining at p10 ($n = 6$). The values are means ± S.E. *D*, expression of hypertrophy marker genes was evaluated by qRT-PCR on p10 hearts ($n = 3–5$).

transcriptional repression function of Jarid2. Gene ontology (GO) term analysis on biological process (BP) showed that organ morphogenesis, ion transmembrane transport, heart development, and muscle contraction were significantly dysregulated (Fig. 5, *C* and *D*). The genes enriched in organ morphogenesis were involved mainly in noncardiac organ development such as lung (*Irx1* and *Irx2*), neuron (*Ntn1*, *Cdh2* and *Gli1*), epidermal stem cell and intestinal stem cell (*Lrig1*), and

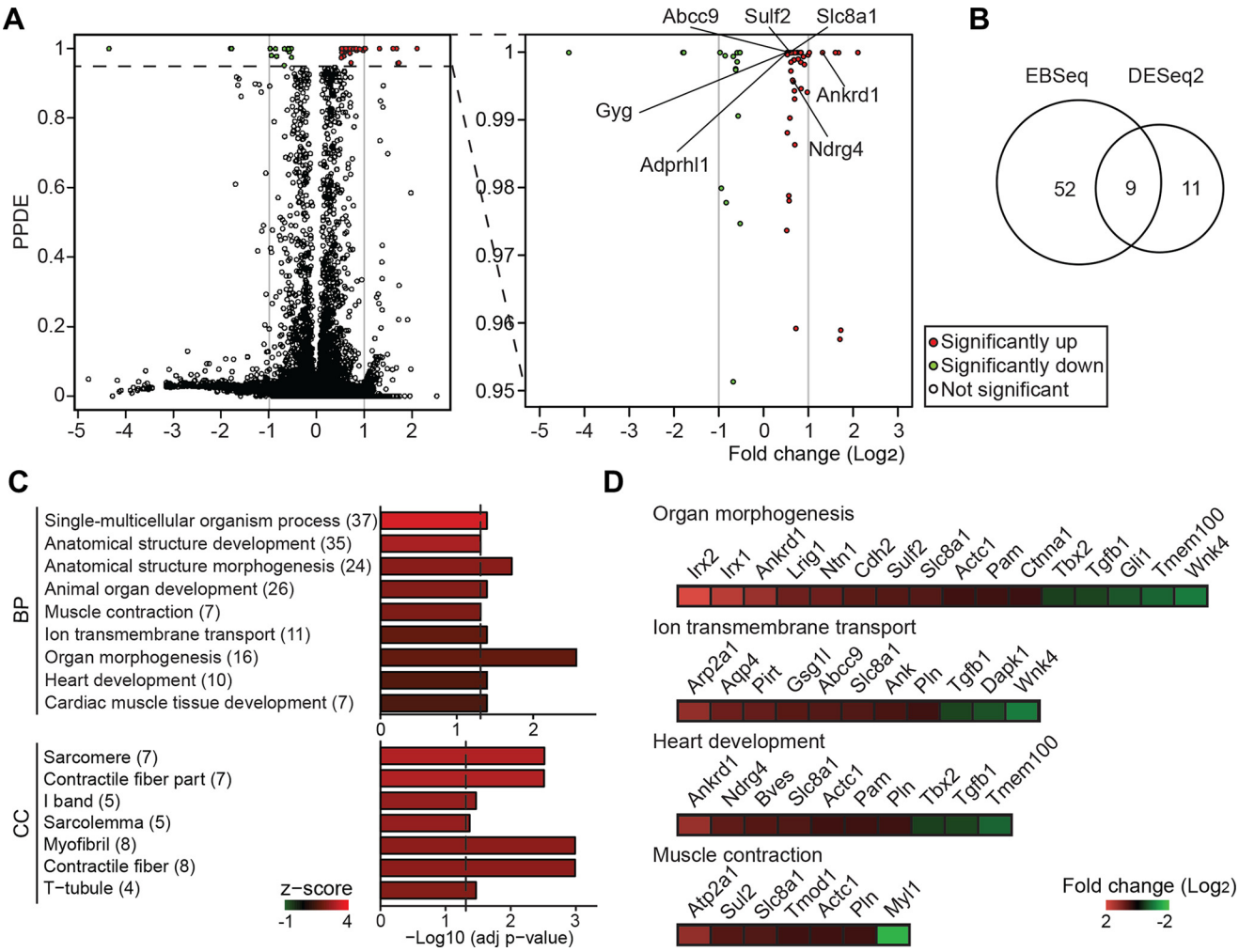

Figure 5. Analyses of gene expression profiling in *Jarid2*$^{\alpha MHC}$ *versus* control hearts at p10. *A*, volcano plots showed differentially expressed genes by EBSeq analyses. 61 genes were dysregulated at a statistically significant level (PPDE > 0.95), which was magnified in the *right panel*. *Gray lines* indicate ±1-fold change. Each gene is indicated by a dot. *B*, Venn diagram demonstrates numbers of DE genes by EBSeq and DESeq2. *C*, GO term analysis was performed with all 72 DE genes to determine significant BP and CC. The *x* axis indicates log-transformed FDR adjusted (*adj*) *p* value, and *dotted lines* indicate adjusted *p* value of <0.05. *Colors* reflect *z* scores. *D*, heat map indicates genes involved in organ morphogenesis, ion transmembrane transport, heart development, and muscle contraction. Increased genes are indicated in *red*, intermediate genes are in *black*, and decreased genes are in *green*.

kidney (*Wnk4*). These results suggest that other organ developmental genes are repressed by Jarid2 in the heart at neonatal stages. Among the 54 up-regulated genes, 5 genes (*Ankrd1*, *Abcc9*, *Actc1*, *Pln*, and *Gyg*) have been shown to be mutated in human cardiomyopathy (2). GO term analysis on cellular component (CC) showed up-regulation of myofibril, contractile fiber, sarcomere, and T-tubule gene pathways in *Jarid2*$^{\alpha MHC}$ hearts at p10. These included increased contractility related genes (*Actc1*, *Slc8a1*, *Abcc9*, *Atp2a1*, *Ankrd1*, *Myl12a*, *Myl1*, and *Tmod1*) prior to hyperperforming hearts at 3 months in *Jarid2*$^{\alpha MHC}$.

To determine potential direct targets of Jarid2, we overlapped 72 DE genes with our Jarid2 ChIP-chip data (23), yielding 15 genes dysregulated in *Jarid2*$^{\alpha MHC}$ hearts whose genomic loci were occupied by Jarid2 (Table S3). Among these, the promoter region of *Gli1*, *Ttll1*, and *Prph* were co-occupied by Jarid2 and H3K27 trimethylation. Gli1, a zinc finger transcription factor, is a modulator and target of hedgehog signaling during embryo development (31). Gli1 has been studied in the generation of vascular smooth muscle cells and regulation of fibrosis (32). Prph is a type III intermediate filament protein presenting in neurons of the mammalian peripheral nervous system and neuroblastoma cells (33). Ttll1 is a member of the tubulin tyrosine ligase superfamily and important for interaction and axoneme motility (34). Other genes occupied by Jarid2 included Tmem100. Because Tmem100 is expressed in endothelial cells and involved in endothelial differentiation (35), it may not be a direct target of Jarid2 in cardiomyocytes. *Tmem100* KO mice are embryonic lethal with cardiovascular failure (36). The sarcoplasmic/endoplasmic reticulum Ca^{2+}-ATPase (SERCA) is a major component of Ca^{2+} cycling, and reduction of SERCA expression and activity have been linked to diastolic dysfunction in failing hearts (37). Although SERCA2a is the major cardiac-specific isoform, SERCA1a overexpression in the heart reveals faster Ca^{2+} transport kinetics by reduction in endogenous SERCA2a levels (37). Thus, increased *Atp2a1* (SERCA1a) levels in *Jarid2*$^{\alpha MHC}$ may impact on SERCA2a activity and thus Ca^{2+} uptake and cardiac contractility.

There were seven DE genes identified by both EBSeq and DESeq2 analyses (Table 2). ADP-ribosylhydrolase–like 1

Table 2
List of seven DE genes identified by both EBSeq and DESeq2 analyses at p10

Gene	Fold change	PPDE	Name
Ankrd1	1.31	1.00	Ankyrin repeat domain 1 (cardiac muscle)
Ndrg4	0.65	1.00	N-myc downstream regulated gene 4
Sulf2	0.61	1.00	Sulfatase 2
Slc8a1	0.58	1.00	Solute carrier family 8 (sodium/calcium exchanger), member 1
Abcc9	0.55	1.00	ATP-binding cassette, subfamily C (CFTR/MRP), member 9
Adprhl1	0.53	1.00	ADP-ribosylhydrolase like 1
Gyg	0.53	1.00	Glycogenin

(Adprhl1) is a member of the ADP-ribosylhydrolase family (38). Although Adprhl1 is enzymatically inactive, it is important for heart chamber outgrowth and myofibril assembly in *Xenopus* embryos (39). The function of Adprhl1 in the mouse heart has not been studied, but elevated *Adprhl1* expression levels may lead to abnormal orientation of myofibrils or contractile defects in *Jarid2*$^{\alpha MHC}$ hearts. Glycogen is a primary form of energy storage in eukaryotes. Glycogenin (Gyg) is a glycosyltransferase that catalyzes the addition of glucose as a primer for glycogen synthesis (40). *GYG1* deficiency has been associated with cardiomyopathies because of an abnormal storage material, polyglucosan in the heart (41). The elevated *Gyg* and *Glycogen branching enzyme 1* (*Gbe1*) in *Jarid2*$^{\alpha MHC}$ hearts suggest that glucose metabolism may be altered. Sodium-calcium exchanger 1 (Slc8a1, NCX1) is an antiporter membrane protein that maintains cytosolic Ca^{2+} homeostasis (42). Dysregulation of *NCX1* in humans is observed in end-stage heart failure, and expression and function of NCX1 are increased during heart failure (42). Therefore, increased *Slc8a1* expression in *Jarid2*$^{\alpha MHC}$ hearts may cause a disruption in Ca^{2+} homeostasis. Abcc9 is an ABC family member and encodes a membrane-associated receptor, SUR2, in the mitochondria and cell membrane. *ABCC9* mutation causes DCM in humans, and KO mice die in the neonatal period with progressive cardiac dysfunction and a failure to transition from fetal to mature myocardial metabolism (43). Abcc9 expression is increased by low oxygen stress mediated by ERK or AKT signaling as a protective effect (44). In *Jarid2*$^{\alpha MHC}$ hearts, elevated *Abcc9* levels imply cardiac dysfunction or defective maturation. Sulfatase 2 (Sulf2) is an extracellular endosulfatase and removes the 6-*O*-sulfate from heparan sulfate. Heparan sulfate is a dynamic molecule in the extracellular matrix and involved in signaling by interacting with growth factors (45). N-myc downstream regulated gene 4 (Ndrg4) is a cytoplasmic protein highly expressed in the heart and brain. Down-regulation of *Ndrg4* leads to hypoplastic hearts in zebrafish, and Ndrg4 expression is down-regulated by Tbx2 in mice (46, 47). In our RNA-seq data, *Tbx2* expression was down-regulated, suggesting that an increase in *Ndrg4* expression may be mediated by reduced *Tbx2* expression. Ankrd1 is a part of the muscle ankyrin repeat protein family and a cardiac-specific stress-response protein. Ankrd1 functions as a transcription co-factor in the nucleus and maintains sarcomere assembly by interacting with titin in the heart (48). Although *Ankrd1* KO mice are viable and display normal heart function, Ankrd1 has been proposed as a potential biomarker for heart failure. *Ankrd1* transcription is directly activated by Nkx2.5 and GATA4, and their transcriptional activities can be repressed by Jarid2 (24). Thus, increased Nkx2.5 and GATA4 activities in *Jarid2*$^{\alpha MHC}$ hearts may activate *Ankrd1* expression. These seven up-regulated genes in *Jarid2*$^{\alpha MHC}$ hearts indicate alterations in expression of critical genes at p10. Interestingly, among the seven genes, four genes (*Gyg*, *Slc8a1*, *Abcc9*, and *Ankrd1*) are heart failure–associated genes.

Gene expression profiling in the Jarid2$^{\alpha MHC}$ *heart during DCM/heart failure*

To determine molecular changes in DCM hearts, we performed RNA-seq on 7-month hearts (Fig. 6). A total of 2375 genes were significantly dysregulated in *Jarid2*$^{\alpha MHC}$ hearts by either EBSeq (Fig. 6*A*) or DESeq2 analysis (Fig. S3*B*). Among those, 1005 genes were common DE genes identified by both analyses (Fig. 6*B*). Major gene ontology of the 1005 genes by BP analysis indicated dysregulation of collagen fibril organization and fatty acid metabolism gene pathways, which consist of mostly up- and down-regulated genes, respectively (Fig. 6*C*). Likewise, the extracellular region and mitochondrion in CC pathways were dysregulated, which consisted of mostly up- and down-regulated genes in *Jarid2*$^{\alpha MHC}$ hearts, respectively. Similarly, fibronectin binding and oxidoreductase activity were identified by molecular function (MF), consisting of up- and down-regulated genes, respectively. Specifically, aerobic metabolism, including fatty acid oxidation and oxidation-reduction process by BP were enriched with down-regulated genes in *Jarid2*$^{\alpha MHC}$ hearts with DCM.

Because highly dysregulated genes in the mutant heart may play important roles in mediating DCM at 7 months, we analyzed 319 dysregulated genes that showed more than 2-fold changes (Fig. 6*D*). Among the 319 DE genes, 128 were down-regulated and 191 were up-regulated. GO term analyses on the down-regulated genes showed action potential, single-organism metabolic process, and regulation of transmembrane transport by BP analysis. The CC analysis indicated sarcolemma and T-tubule, and MF analysis showed voltage-gated ion channel activities. The up-regulated genes were mainly involved in extracellular region (84 of 191). Interestingly, PI3K-Akt signaling pathway was identified by KEGG analyses, which included many extracellular matrix genes (*Col1a1*, *Col1a2*, *Col3a1*, *Col5a2*, *Col6a3*, *Col11a1*, *Cdkn1a*, *Gng8*, *Itga11*, *Lpar3*, *Myc*, *Spp1*, *Tnc*, and *Thbs4*). Additionally, heart failure–associated genes or extracellular matrix genes were up-regulated, including *Tissue inhibitor of metaolloprotease-1* (*Timp1*), *A disintegrin and metalloproteinase with thrombosponding repeats-like 2* (*Adamtsl2*), and *Small proline-rich repeat protein 1a* (*Sprr1a*). Timp1 is a collagenase inhibitor (49). Adamtsl2 mutation causes geleophysic dysplasia with cardiac defects, including ventricular septal defect and thickened and nonstenotic aortic valve (50). Sprr1a is overexpressed in myocytes after mechanical stress and may prevent the myocytes against permanent damages (51). Therefore, *Jarid2*$^{\alpha MHC}$ hearts exhibited increases in stress-response genes and fibrosis related genes.

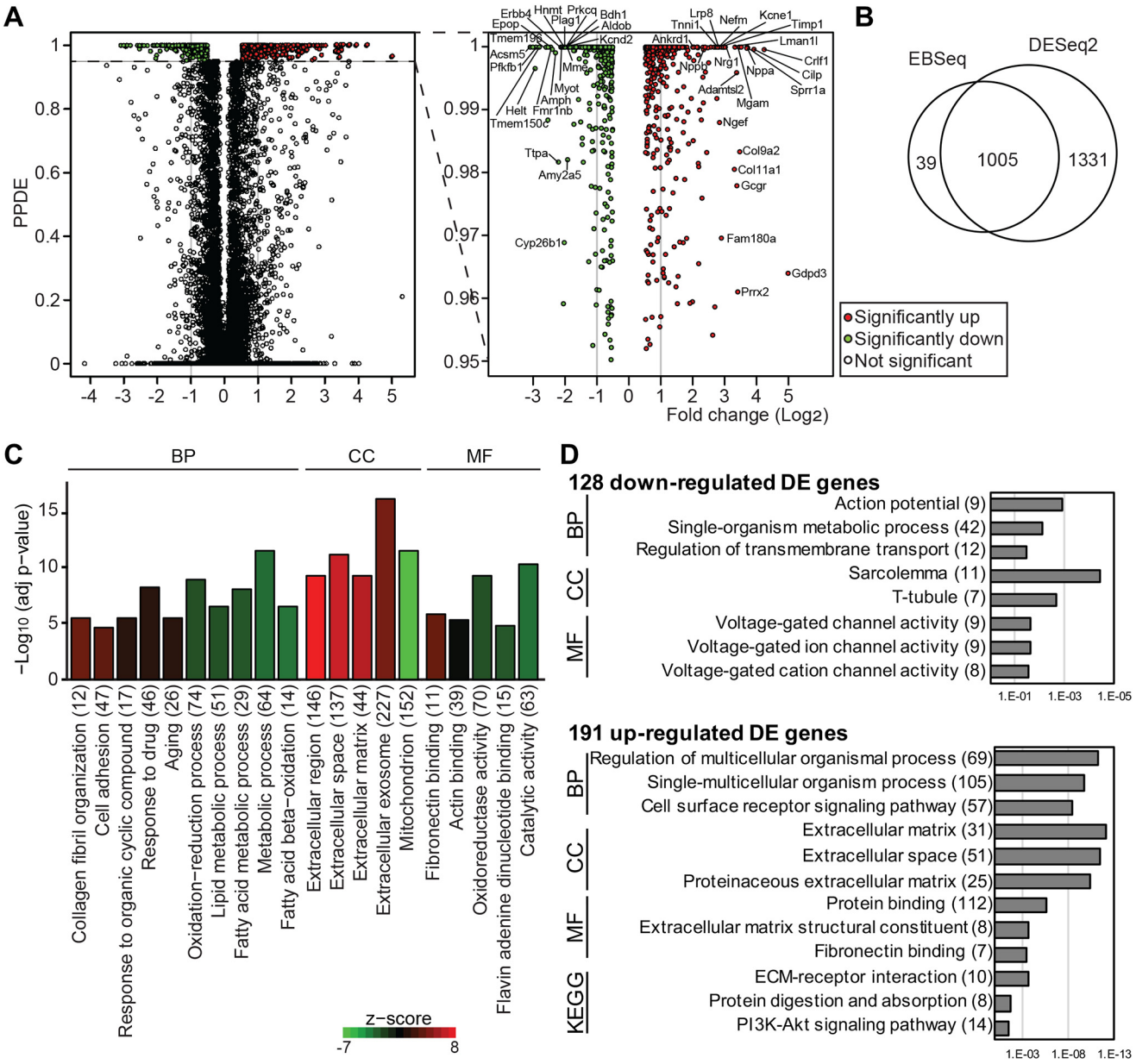

Figure 6. Analyses of gene expression profiling in *Jarid2*$^{\alpha MHC}$ *versus* control hearts at 7 months. *A*, volcano plots showed DE genes by EBSeq. 1044 genes were statistically significant (PPDE > 0.95), indicated by *dotted line*, and magnified in the *right panel*. All genes are indicated by *dots*. *B*, Venn diagram demonstrates numbers of differentially expressed genes by EBSeq and DESeq2. 1005 genes were common DE genes in EBSeq and DESeq2. *C*, GO term analysis was performed with 1005 genes. The top ten BPs and top five CCs and MFs are indicated (FDR adjusted (adj) *p* value of <0.05). *D*, GO term analysis was performed with 319 DE genes that showed greater than 2-fold changes. All significant categories were shown for down-regulated genes, and the top three significant categories were shown for up-regulated genes (FDR adjusted *p* value < 0.05). *KEGG*, Kyoto Encyclopedia of Genes and Genomes.

Jarid2 is required for myocardial maturation

Next, we determined genes that are continuously dysregulated at both p10 and 7 months in the mutant heart to increase mechanistic insights into the Jarid2 function and DCM progression. Our RNA-seq data indicated that only 12 genes were significantly dysregulated in *Jarid2*$^{\alpha MHC}$ hearts at both p10 and 7 months (Fig. 7*A*). Most of these genes (*Lpar3*, *Sulf2*, *Gsg1l*, *Irx2*, *Pam*, *Ankrd1*, *Gyg*, *Lnx1*, and *Adprhl1*) continued to be up-regulated in *Jarid2*$^{\alpha MHC}$ hearts at p10 and 7 months compared with controls, implying that Jarid2 may function in suppressing these genes in normal hearts. Lpar3 is a receptor for lysophosphatidic acid belonging to the G protein–coupled receptor family and is expressed in the myocardium during postnatal maturation stages (52). Pam is a membrane protein containing peptidylglycine α-hydroxylating monooxygenase and α-amidating enzymes (53). Pam has been studied in the atrium for α-amidation and pro-ANP packaging in secretory granules (54). Lnx1 is an E3 ubiquitin ligase that mediates the ubiquitination and degradation of Numb and also ubiquitinates ErbB2 receptors in Schwann cells for the maturation (55). Therefore, increased Lnx1 might regulate Nrg1–ErbB signaling pathways in *Jarid2*$^{\alpha MHC}$ hearts. Gsg1l is a transmembrane auxiliary subunit of α-amino-3-hydroxy-5-methyl-4-isoxazolepropionic acid receptors, which are ionotropic glutamate receptors in the central nervous system (56). *Lectin galactoside-binding soluble 4* (*Lgals4*) and *With no lysine kinase 4* (*Wnk4*) were

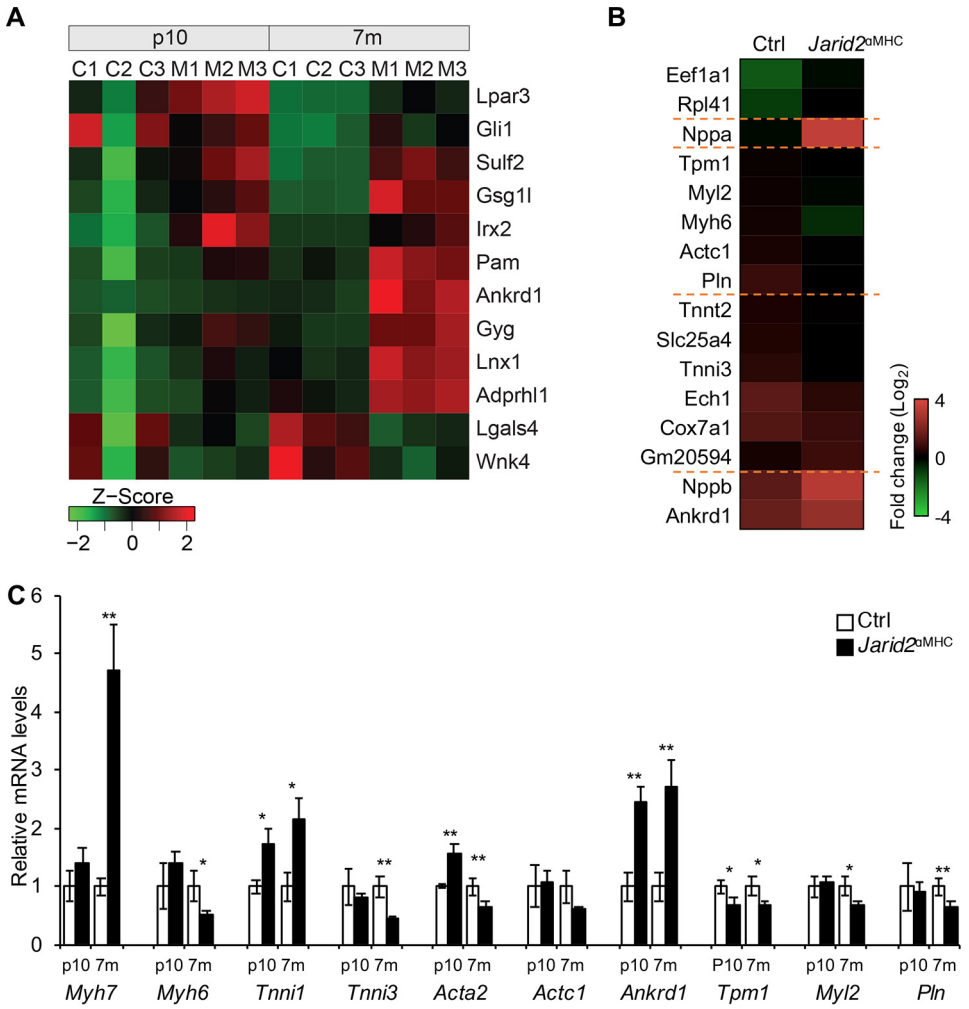

Figure 7. Jarid2 was required for myocardial maturation. *A*, the heat map shows statistically significantly dysregulated genes in *Jarid2*$^{\alpha MHC}$ at both p10 and 7 months (m). Only 12 genes were identified as dysregulated genes among 72 genes and 2375 genes at p10 and 7 months, respectively. *B*, the heat map consists of 16 genes identified by time-dependent differential gene expression. 16 genes were statistically significant in our analysis, and the fold changes from p10 to 7 months are presented by *colors*. *C*, qRT-PCR was performed to determine expression levels of DE genes in p10 and 7-month hearts (n = 3–5). *Ctrl*, control.

expressed higher in control hearts at p10 and 7 months compared with mutants. *Gli1* was down-regulated at p10 but up-regulated at 7 months in mutant hearts.

Because the heart undergoes postnatal development, we reasoned that comparing normal age-dependent changes in gene expression patterns from p10 to 7 months in control *versus* mutant hearts may provide important information to identify developmental defects in the mutant heart (Fig. 7*B*). There were 16 genes showing significantly different time-dependent patterns between control and *Jarid2*$^{\alpha MHC}$ hearts. In *Jarid2*$^{\alpha MHC}$ hearts, *Eukaryotic elongation factor 1* (*Eef1a1*), *Nppa*, *Nppb*, and *Ankrd1* were significantly increased compared with controls, which are linked to heart failure. In contrast, metabolic process–related genes, such as *Cytochrome c oxidase subunit 7a1* (*Cox7a1*) and *Enoyl CoA hydratase 1* (*Ech1*), were down-regulated in mutant hearts compared with controls. Cox7a1 is a complex of the mitochondrial respiratory chain and a heart and skeletal muscle-specific enzyme. *Cox7a1* KO mice develop DCM with reduced Cox activities in the muscle (57). Ech1 is the second enzyme of mitochondrial fatty acid β-oxidase pathways and associated with cell growth and apoptosis (58).

Interestingly, *Ankrd1* and *Nppb* expression levels were slightly up-regulated in control hearts from p10 to 7 months (1.6- and 1.4-fold, respectively), even though these genes were highly up-regulated in *Jarid2*$^{\alpha MHC}$ hearts (2.5- and 3.2-fold, respectively). Contractile gene expression (*Tpm1*, *Myl2*, *Myh6*, *Actc1*, *Pln*, *Tnnt2*, and *Tnni3*) was increased in control hearts from p10 to 7 months, whereas expression of these genes was not increased as much in *Jarid2*$^{\alpha MHC}$ hearts. Indeed, expression levels of *Tpm1*, *Myl2*, *Myh6*, *Actc1*, and *Pln* were reduced from p10 to 7 months in *Jarid2*$^{\alpha MHC}$ hearts. These results suggest that Jarid2 is important to increase or maintain the expression of contractile genes for mature cardiomyocytes.

To analyze sarcomere gene expression, we examined expression levels of fetal isoforms such as *Myl7*, *Tnni1*, and *Acta2* by qRT-PCR on p10 and 7-month hearts (Fig. 7*C*). In general, these fetal genes are switched to the adult forms during myocardial maturation (59). *Tnni1* and *Acta2* were significantly increased in the mutant neonatal heart. Ankrd1 is expressed at a higher level in the embryonic heart than the adult heart (48). *Ankrd1* expression was continuously increased in p10 and 7-month *Jarid2*$^{\alpha MHC}$ hearts. *Myh7*, a fetal isoform, was only

increased at 7 months, which is a hallmark for heart failure, namely "fetal gene re-expression." *Tpm1*, *Myl2*, and *Pln* are important contractile genes that are increased as the heart matures, and dysregulations of these genes are linked to DCM (60). However, these genes were down-regulated in 7-month *Jarid2*$^{\alpha MHC}$ hearts, although *Myl2* and *Pln* expression levels were not altered at p10 (Fig. 7*C*). These data suggest that Jarid2 is necessary to repress expression of fetal genes and maintain mature genes in the adult heart.

Dysregulation of Nrg1–ErbB4 signaling pathway in Jarid2-deficient hearts

We have previously shown that Notch1–Nrg1–ErbB signaling pathways were increased in *Jarid2* KO embryonic hearts (20). Myocardial-specific induction of ErbB2 causes cardiac hypertrophy and dedifferentiation of the cardiomyocytes mediated by ERK and AKT signaling pathways (15). In our RNA-seq data, *Nrg1* was highly up-regulated, whereas *ErbB4* was down-regulated in *Jarid2*$^{\alpha MHC}$ hearts at 7 months (Fig. 6*A*). Therefore, we examined whether the altered immature gene expression is correlated with Nrg1–ErbB signaling. First, we determined the expression levels of *Nrg1* and *ErbB4* by qRT-PCR (Fig. 8, *A* and *B*). Interestingly, *Nrg1* expression was continuously increased in *Jarid2*$^{\alpha MHC}$ hearts from 1 to 7 months (DCM). In contrast, *ErbB4* expression in the myocardium was temporarily increased at p10 but down-regulated by 7 months in *Jarid2*$^{\alpha MHC}$ hearts. Because Nrg1–ErbB signaling activates AKT and ERK pathways (15), we examined ErbB4 protein levels and downstream signals (Fig. 8, *C* and *D*). ErbB4 protein expression was increased in *Jarid2*$^{\alpha MHC}$ hearts compared with controls at p10, correlating with mRNA levels. Phospho-AKT and phospho-ERK1/2 expression levels were significantly elevated, whereas total AKT and ERK1/2 expression levels were not changed. To determine whether increased ErbB4 signaling pathways directly regulate fetal gene expression, isolated cardiomyocytes from control and *Jarid2*$^{\alpha MHC}$ hearts were incubated in ErbB inhibitors. Under the vehicle-treated control condition, *Tnni1* and *Acta2* expression levels were significantly higher in *Jarid2*$^{\alpha MHC}$ *versus* control hearts (Fig. 8*E*). However, these increases were normalized to control levels by the treatment with an ErbB receptor inhibitor (Fig. 8*F*). These results suggest that Jarid2 may mediate transition from fetal to adult gene expression via ErbB4 signaling pathways during neonatal stages. Further experiments are required to determine whether Jarid2 is a direct regulator of ErbB4 signaling and to examine *in vivo* effects of blocking ErbB signaling on gene regulation in the mutant heart.

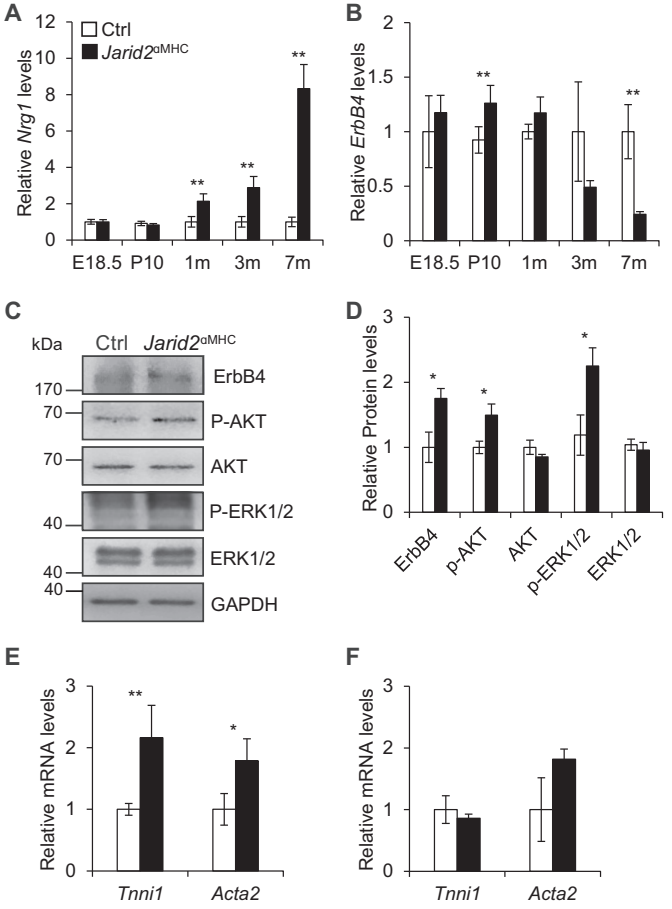

Figure 8. ErbB4 was up-regulated in *Jarid2*$^{\alpha MHC}$ hearts at p10. *A* and *B*, *Nrg1* (*A*) and *ErbB4* (*B*) expression levels were determined by qRT-PCR on the heart at different ages. The expression levels in *Jarid2*$^{\alpha MHC}$ hearts were normalized to each control (*Ctrl*) level (n = 3–5). *C*, Western blotting was performed to determine ErbB4, AKT, and ERK pathways on p10 hearts. *D*, the graph showed the protein levels of ErbB4, AKT, and ERK by standardization to GAPDH and normalization to control levels. *E* and *F*, qRT-PCR was performed on isolated cardiomyocytes from new born hearts, which were incubated in vehicle (*E*) or the ErbB inhibitor AG1478 (5μM) (*F*) (n = 3–5).

Discussion

In the present study, the molecular and developmental functions of Jarid2 were determined in the postnatal heart. *Jarid2*$^{\alpha MHC}$ mice exhibited DCM with contractility defects, leading to premature death at approximately 6–9 months of age. Because Jarid2 expression was maintained in neonatal hearts but significantly decreased thereafter, we reasoned that Jarid2 functions critically in neonatal hearts. These studies will increase our understanding on the molecular etiology of DCM. Thus, we analyzed gene expression profiling at p10 (neonatal) and 7 months (DCM) hearts. At p10, dysregulated genes in *Jarid2*$^{\alpha MHC}$ hearts represented mainly heart development and muscle contraction pathways, and heart failure-related genes were significantly elevated, although the mutant heart morphology appears normal. At 7 months, the metabolic process and ion channel activity pathways were enriched with down-regulated genes, and extracellular matrix component genes were up-regulated in *Jarid2*$^{\alpha MHC}$ hearts. These data indicate that Jarid2 is important for regulating genes for neonatal heart development and muscle contraction at p10, even when cardiac morphology and function seem normal (Fig. 9). These early changes in gene expression may contribute to hyperfunctioning hearts, and lethal DCM at 7 months. To determine whether Jarid2 plays important roles in maturation of cardiomyocytes postnatally, we analyzed gene expression patterns from p10 to 7 months. In normal hearts, sarcomere- and contractile-associated genes were up-regulated from p10 to 7 months in an age-dependent manner, whereas these genes were not sufficiently increased with age in *Jarid2*$^{\alpha MHC}$ hearts. These data suggest that Jarid2 is essential in cardiomyocyte maturation and normal sarcomere development.

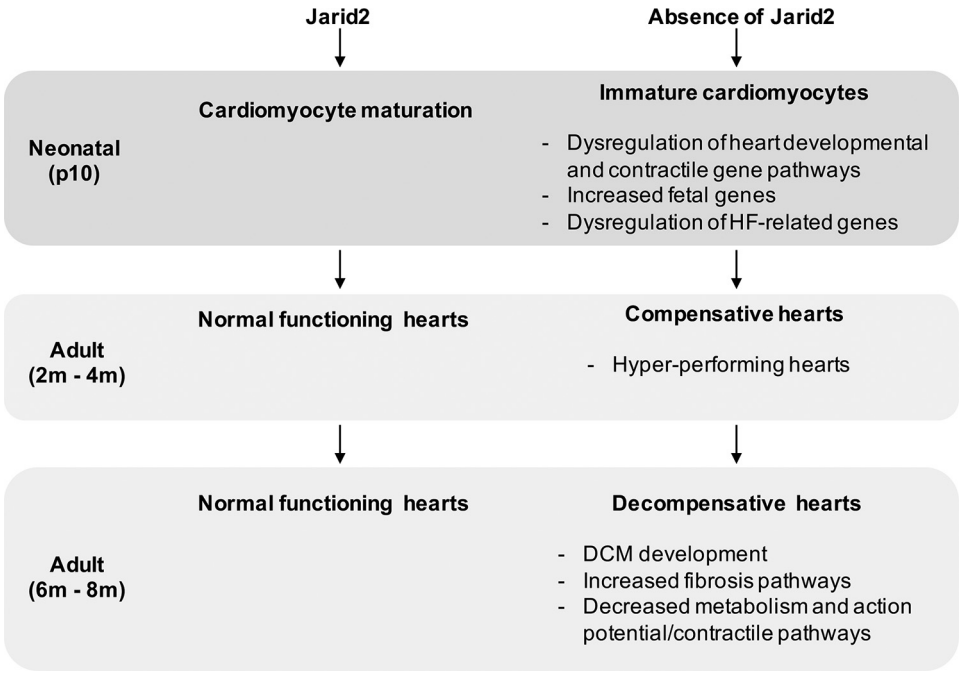

Figure 9. Summary of Jarid2 function in the postnatal heart. Jarid2 plays important roles in cardiomyocyte maturation during neonatal stages and inhibiting DCM development. *HF*, heart failure.

Jarid2 deletion mice by *αMHC*::*Cre* survived to adulthood and showed DCM, whereas those by *Nkx2.5*::*Cre* died with cardiac malformations within 1 day after birth (21). Although both Cre lines are cardiac-specific, *Nkx2.5*::*Cre* expresses Cre earlier than *αMHC*::*Cre* and is considered as cardiac progenitor-specific (28), whereas *αMHC*::*Cre* as differentiated cardiomyocyte-specific. Accordingly, *Nkx2.5*::*Cre* expression domains include noncardiomyocytes such as endocardial cells. However, it has been reported that *Nkx2.5*::*Cre* did not delete certain genes in the endocardium (61). Jarid2 deletion mice by *Nkx2.5*::*Cre* also showed that Jarid2 was expressed and functional in the endocardium (21), supporting the critical function of Jarid2 in the cardiomyocyte progenitors during early development. *αMHC*::*Cre* begins expressing Cre in embryonic cardiomyocytes. Thus, one cannot exclude a possibility that some cardiac defects in *Jarid2*$^{\alpha MHC}$ mice may be embryonic origin. The adult function of Jarid2 can be determined by time-dependent cardiac-specific deletion of Jarid2, such as tamoxifen-induced deletion after birth. If an adult conditional deletion of Jarid2 produces no phenotype, heart failure in *Jarid2*$^{\alpha MHC}$ mice may have congenital origins. However, given that the neonatal heart of *Jarid2*$^{\alpha MHC}$ mice is morphologically normal and shows a small number of dysregulated genes at p10 and that the αMHC promoter becomes stronger after birth, embryonic defects may not be a major contributor in DCM progression.

Jarid2 is an important transcription factor in heart development. *Jarid2* KO mice develop congenital cardiac defects such as thin myocardium, hypertrabeculation, and ventricular septal defects during embryonic stages (27). Although Jarid2 is an enzymatically inactive member of the JMJ histone demethylase family, Jarid2 can function as an epigenetic regulator by recruiting histone methyltransferases in the developing heart (22). However, the function of Jarid2 in the adult heart is not fully understood. The RNA-seq data at p10 were overlapped with our Jarid2 ChIP-chip data from the developing heart (23) to determine potential targets of Jarid2 (Table S3). Among the 72 DE genes, Jarid2 occupies the promoters of the 15 genes, which are potential direct targets of Jarid2. Contractile-related genes (*Ttll1* and *Atp2a1*) were up-regulated in mutant hearts, correlating with the transcriptional repression function of Jarid2. Cell proliferation and differentiation-related genes (*Tmem100*, *Gli1*, *Tgfb1*, and *Egfl7*) were down-regulated in mutant hearts, implying potential transcriptional activation functions of Jarid2. However, because ChIP-chip assays were performed using embryonic hearts, this overlapping has limitations caused by age and environmental differences. Further investigation into Jarid2 occupancy in the postnatal heart would be important to determine direct targets of Jarid2. In *Jarid2*$^{\alpha MHC}$ mice at p10, cardiac morphology is overtly normal, yet altered expression of genes involved in ion transmembrane transport and muscle contraction has already occurred. This suggests that dysregulation of these genes is not sufficient to develop morphological and functional defects at p10 but may be causal to hyperfunctioning hearts at 3 months and maladaptation to DCM at 7 months. Although Jarid2 expression is significantly reduced within 1 month of birth, DCM was not manifested until much later in the mutant heart. It is plausible that dysregulation of gene expression during neonatal stages may be permanent, leading to DCM later in life. Alternatively or concomitantly, compensatory mechanisms may contribute to hyperperforming heart in the mutant, followed by pathological remodeling caused by cumulative compensation and chronic stimuli. Given that Jarid2 expression level is not significant in the adult heart, it would be interesting to determine whether epigenetic changes on genomic loci of the DE genes at p10 are maintained later in the adult heart by performing ChIP assays.

Jarid2$^{\alpha MHC}$ mice exhibited DCM and increased gene expression involved in collagen fibril organization and extracellular

matrix remodeling, indicating increased fibrosis, a common feature of pathological remodeling in the failing heart. Cardiac fibrosis can cause disruption of myocardial architecture and impairment of systolic and diastolic function (62, 63). *Jarid2*$^{\alpha MHC}$ hearts showed dysregulated collagen synthesis (*Col6a3*, *Col1a2*, *Col5a2*, *Col3a1*, *Col1a1*, *Col14a1*, *Col11a1*, and *Col9a2*). In addition, genes involved in extracellular matrix degradation were dysregulated such as metalloproteases (*Mmp19*, *Mmp2*, *Mmp14*, *Mmp23*, *Adamts7*, *Adamts3*, *Adamts2*, *Adamtsl2*, *Adam22*, and *Adam 11*) and metalloproteases inhibitor (*Timp1*). Secreted factors regulating fibrosis (*Fgf11*, *Fgf9*, *Ptn*, and *Fstl3*) were also dysregulated in *Jarid2*$^{\alpha MHC}$ hearts. Interestingly, Serpin isoforms (*Serpinf1*, *Serpina3n*, *Serpine1*, and *Serpinb1c*) were highly increased in *Jarid2*$^{\alpha MHC}$ hearts at 7 months. Serpins are serine protease inhibitors, which regulate anti-fibrinolysis. Serpine1 (PAI1) inhibits the Mmp activity involved in fibrosis (64). Together, these findings suggest that increased fibrosis in *Jarid2*$^{\alpha MHC}$ hearts is mediated by dysregulation of collagen, Mmp, and Serpin expression.

The adult heart produces 90% of its ATP using fatty acid oxidation. However, this energy metabolism is changed to glycolysis in the failing heart (65). *Jarid2*$^{\alpha MHC}$ hearts at 7 months displayed a reduction of fatty acid metabolic process. The peroxisome proliferator–activated receptor (PPAR) pathway is a key regulator in heart metabolism, which is inhibited in DCM mouse models (66). PPAR downstream signaling was significantly reduced in *Jarid2*$^{\alpha MHC}$ hearts at 7 months (*Slc27a1*, *Acadl*, *Esrrb*, and *Ppargc1a*). However, this pathway was not altered in p10 hearts, suggesting that reduced fatty acid metabolism is a result of DCM pathogenesis. PPARγ coactivator 1α (PGC1α, Ppargc1a) regulates mitochondrial biogenesis and oxidative phosphorylation in the heart (66), implying that mitochondrial function is perturbated in *Jarid2*$^{\alpha MHC}$ hearts (Fig. 6*C*). Glucose metabolism process was not identified as a significantly dysregulated pathway in *Jarid2*$^{\alpha MHC}$ hearts at 7 months. However, RNA-seq data showed decreases in glycolysis- and gluconeogenesis-related genes (*Ldhb*, *Galm*, *Acss1*, *Aldob*, *Fbp2*, and *Aldh9a1*) and increases in glucose synthesis enzymes (*Ptges3*, *Prkag3*, *Gck*, and *Gyg*), implying a shift from aerobic metabolism to nonoxidative glucose metabolism in *Jarid2*$^{\alpha MHC}$ hearts at 7 months.

In mouse models of heart failure, Nrg1 expression is higher, whereas ErbB2 and ErbB4 expression levels are decreased during the transition from compensatory hypertrophy to heart failure (16). Nrg1 improves heart function and prevents cardiac fibrosis in animal models and heart failure patients (16). Increases in Nrg1 and ErbB4 expression correlate with increases in contractility in animal models of heart failure (17). It is interesting that in our study, *Nrg1* expression was increased from 1 month, which was much earlier than the onset of DCM. Thus, it is plausible that early increases in *Nrg1* lead to the hyperperforming heart at 3 months. Elevated levels of *Nrg1* and decreased *ErbB4* in 7 months *Jarid2*$^{\alpha MHC}$ hearts correlate with a general heart failure phenotype. Induction of constitutively active ErbB2 in neonatal hearts causes re-entry of cardiomyocytes into the cell cycle mediated by Nrg1 (15), and activation of Nrg1 and ErbB4 induces proliferation of differentiated cardiomyocytes (67). Although *ErbB4* expression was altered in *Jarid2*$^{\alpha MHC}$ hearts at p10, the cell proliferation was not changed, implying that an increase in *ErbB4* expression is not sufficient to induce cell proliferation. Because *Nrg1* expression was up-regulated in *Jarid2*$^{\alpha MHC}$ hearts from 1 month, increased *Nrg1* may serve as an early indicator of cardiomyopathy.

Ankrd1 was highly increased in neonatal as well as failing hearts of *Jarid2*$^{\alpha MHC}$ mice. Transgenic mice with *Ankrd1* overexpression display normal cardiac morphology (48), and the function of increased Ankrd1 in the adult heart is controversial. Ankrd1 can mediate adaptive and protective responses against pathological damages (68, 69). In contrast, Ankrd1 can accelerate the progression to hypertrophy (70–72). It is possible that increased *Ankrd1* at p10 plays a protective role to maintain normal heart morphology and functions, which may lead to the hyperfunctioning heart at 3 months. It is unclear whether chronic overexpression of *Ankrd1* is protective or accelerates the progression of DCM in *Jarid2*$^{\alpha MHC}$ mice at 7 months. Because *Ankrd1* expression is already increased at p10, which is much earlier than the onset of DCM, it may serve as an early sensitive marker of cardiomyopathy. It would be interesting to determine the role of early increases in *Nrg1* and *Ankrd1* in DCM pathogenesis in *Jarid2*$^{\alpha MHC}$ mice.

In our RNA-seq data, only 72 genes were differentially expressed in p10 mutant hearts compared with controls, whereas 2375 genes were dysregulated at 7 months, suggesting that *Jarid2*$^{\alpha MHC}$ hearts are not severely perturbed in neonatal stages. However, of the 72 genes, 12 genes were also differentially expressed at 7 months, of which 2 genes were maintained down-regulation and 9 genes were maintained up-regulation in *Jarid2*$^{\alpha MHC}$ hearts *versus* controls, implying that Jarid2 function is critical in regulating expression of certain genes from the neonatal to adult stages. Moreover, in control hearts, sarcomere and contractile-associated genes were increased in an age-dependent manner (Fig. 7, *B* and *C*), whereas these genes were not increased in *Jarid2*$^{\alpha MHC}$ hearts.

Time-dependent gene expression profiling data have been reported in another DCM mouse model with a phospholamban (PlnR9C) mutation (66). By comparing the published dysregulated genes in pre-DCM mutant hearts with our data at p10, we identified the dysregulated genes common to both hearts. These include *Ttll1*, *Myl1*, *Gyg*, and *Ankrd1* (in cardiomyocytes) and *Ampd3*, *Atp2a1*, *Kctd17*, *Sulf2*, and *Tgfb1* (in noncardiomyocytes). Interestingly, a group of genes that are decreased in PlnR9C mice at the DCM stage (*Abcc9*, *Ank*, *Esrrg*, *Irx1*, *Mdh1*, *Pln*, *Suclg2*, and *Ttll1*) was up-regulated in *Jarid2*$^{\alpha MHC}$ hearts at p10 prior to the development of DCM. Some genes increased in PlnR9C mice at the DCM stage were increased in p10 *Jarid2*$^{\alpha MHC}$ hearts, such as *Gbe1*, *Ndrg4*, *Gyg*, and *Ankrd1*. Thus, Jarid2 controls the gene expression at neonatal stages, which may contribute to DCM development in adulthood. Further studies are necessary to determine whether up-regulation of these DCM-related genes at p10 leads to DCM in mutant hearts. Further investigation into the ability of *Jarid2*$^{\alpha MHC}$ mice respond to pathological stresses would be interesting. Together, we demonstrate for the first time that Jarid2 plays crucial roles in the development of postnatal hearts, which will provide an important framework for understanding the molecular and genetic basis of cardiomyopathy in humans.

Experimental procedures

Animal husbandry and echocardiography

All studies using animals were conducted in accordance with University of Wisconsin Research Animal Resource Center policies and the National Institutes of Health Guide for the Care and Use of Laboratory Animals. All animal research has been approved by an Institutional Animal Care and Use Committee (protocol M005971). All mice were littermate or age-matched controls and mutants. The studies were not blinded. Herein, *Jarid2* conditional deletion mice using *αMHC*::*Cre* mice (28), *αMHC*::*Cre/+; Jarid2f/f*, were designated as *Jarid2*$^{\alpha MHC}$. To generate *Jarid2*$^{\alpha MHC}$ mice, females homozygous for the floxed *Jarid2* allele (*Jarid2f/f*) (29) were mated with *αMHC*::*Cre/+; Jarid2f/+* males. *αMHC*::*Cre/−; Jarid2f/f* mice were used as the control throughout this study. All mice employed in this study were bred to a mixed 129/Svj and C57BL/6 genetic background, and genotyping was performed by PCR as described (29).

Transthoracic echocardiography was performed on mice under 1% isoflurane gas anesthesia using a Visual Sonics 770 ultrasonograph with a 30 or 40-MHz transducer (RMV 707B) as described previously (9). Two-dimensionally guided M-mode images of the LV and Doppler studies were acquired at the tip of the papillary muscles. All cardiac parameters were measured over at least three consecutive cycles and analyzed as shown in Table 1. Fractional shortening was calculated as (LVID;d − LVID;s)/LVID;d × 100.

Western blotting, cardiomyocyte culture, and qRT-PCR

To determine the protein levels, Western blotting was performed using heart extracts as described previously (20). The primary antibodies used were anti-Jarid2 peptide antibodies (20), anti-ErbB4 (Santa Cruz, sc283), anti-phospho-AKT (CST, 3787), anti-AKT (CST, 4685), anti-phospho-ERK1/2 (CST, 9106), anti-ERK1/2 (CST, 9102), anti-Cleaved-Caspase3 (CST, 9664), and anti-GAPDH (Millipore, MAB374) followed by horseradish peroxidase–conjugated secondary antibodies (Santa Cruz, sc2005 and sc2004). Protein bands were detected by chemiluminescence (Thermo Scientific) and quantitated with National Institutes of Health ImageJ software. Cultured primary cardiomyocytes were prepared from newborn (p1) mouse hearts as we described (73), yielding ~70% cardiomyocytes under our culture condition. The cells were plated in Dulbecco's modified Eagle's medium with 10% horse serum and 5% fetal bovine serum. ErbB inhibitor, AG1478 (5 μM, Sigma), or vehicle (1:1 ratio of methanol and DMSO) as control was added to serum-free medium for 2 days for qRT-PCR experiments.

qRT-PCR was performed as we described (20). Briefly, mRNAs extracted from mouse ventricles were reverse transcribed to cDNA using cDNA synthesis kit (Thermo Fisher) followed by qRT-PCR using FastStart SYBR Green Master (Roche) on a Bio-Rad iCycler. The appropriate primers for each gene are listed in Table S4. All primers were thoroughly evaluated by melt curve analysis to ensure the amplification of a single, desired amplicon. All samples were assayed in duplicate with nearly identical replicate values. The data were generated using the standard curve method and normalized to 18S expression. qRT-PCR data were analyzed by the RQ analysis algorithm (Bio-Rad).

Histology, Lac Z staining, and immunohistochemistry

H&E staining (27), and immunohistochemistry were performed on paraffin-embedded sections as described (20). Briefly, tissue sections were incubated with primary antibodies, anti-Jarid2, anti-MF-20 (DSHB, MF20), anti-Ki-67 (Abcam, ab15580), and anti-phospho-H3 (Millipore, 06-750). Alexa dye-conjugated secondary antibodies (Invitrogen) or DAB substrate kit (Vector Laboratories, sk-4100) was used for visualization. LacZ staining was performed on hearts of heterozygous mice containing a gene trap insertion of *LacZ* into the *Jarid2* locus as described previously (27). Briefly, the hearts were isolated and fixed with 0.5% glutaraldehyde at different ages. The cryosections were incubated in X-gal staining solution at 37 °C for 2 h. Cardiomyocyte CSA was measured in WGA (Invitrogen) stained cardiac sections as described (9). CSA was evaluated in at least 200 cardiomyocytes per animal from identical areas of the left ventricular wall. Cardiomyocytes only showing the nucleus in the middle of octagonal cell shape were included in the measurements. Hoechst dye was used for counterstaining of nuclei. The images were taken using a Zeiss Axiovert 200 microscope and an AxoiCam HRc camera. Picrosirius staining for collagen were performed as described (9, 27).

Analyses of RNA-seq data

RNA-seq experiments were performed at the University of Wisconsin Biotechnology Center (74). Briefly, total RNA was extracted from control or *Jarid2*$^{\alpha MHC}$ hearts at p10 or 7 months. For each group, three biological replicates were prepared. Total RNA samples were synthesized into double-stranded cDNA using SuperScript II reverse transcriptase (Invitrogen) and random primers. The cDNA products were ligated to Illumina adapters and amplified. Quality and quantity of the finished libraries were assessed using an Agilent HS DNA or DNA1000 chip (Agilent Technologies) and Qubit® dsDNA HS assay kit (Invitrogen), respectively. Single-end 100-bp sequencing was performed on an Illumina HiSeq2500 sequencer and analyzed using the standard Illumina Pipeline, version 1.8.2. Following quality assessment, the sequencing reads were aligned to reference sequences of transcriptome from NCBI (GRCm38.p6) using Bowtie v 1.1.2 allowing two mismatches (75). Based on the aligned reads, countable values, expected counts, and transcript per million (TPM) for each transcript were estimated by RSEM v 1.3.0 (76). The statistical programming language R (version 3.4.4) was used for further data processing.

RNA-seq data analyses were performed as described (30). DESeq2 was used to identify DE genes with high precision and accuracy. Genes that have false discovery rate (FDR) adjusted p value < 0.05 were considered as DE genes with statistical significance. DE genes were displayed in an MA plot. Another DE analytic tool, EBSeq, was used to identify DE genes based on the Bayesian empirical approach. Genes with value of posterior probability of differential expression (PPDE) of >0.95 were considered as significantly DE genes that were plotted on a volcano plot. GO term enrichment on DE genes was assessed

using the Database for Visualization and Integrative Discovery (DAVID) functional analysis software (https://david.ncifcrf.gov) (77, 78). GO terms were obtained from three categories: BP, CC, and MF. Significance of enrichment for each GO term was determined by FDR adjusted p value < 0.05 based on EASE scores (79) and modified Fisher's exact test. Significant GO terms in enrichment were visualized using R packages. The RNA-seq data have been submitted to the Gene Expression Omnibus under accession no. GSE118945.

Time-dependent differential gene expression analysis

We applied a simple and novel technique to rank DE genes by directly comparing the degree of changes of their TPM value under different conditions in terms of geometric calculation over time. For each gene, we compared changes of its TPM values from p10 to 7 months between control and *Jarid2*$^{\alpha MHC}$ hearts. To quantify the degree of changes, we calculated an angle between two 2D vectors: one vector for *Jarid2*$^{\alpha MHC}$ and the other vector for the control. The y value of the starting point in the vectors was obtained from the TPM value at p10, and the y value of the ending point is from the TPM value at 7 months. The difference between the x values of the two points in a vector was adopted from the maximum difference of y values. We calculated an outer product of the two vectors to obtain the angle, which indicates the degree of change. To detect significant genes, we fit the angle data into Gaussian distribution and filter angles with p values < 0.05. The significant genes were visualized by heat map using TPM values.

Statistical analysis

The data represent the averages of three to five replicates and S.E. The replicate numbers are indicated in the text. Significance was determined by Student's t test, and differences are considered significant with a p value of ≤ 0.05 (*) and very significant with a value of $p \leq 0.01$ (**).

Author contributions—E. C. and Y. L. conceptualization; E. C., H. K., and D.-K. K. resources; E. C. and Y. L. data curation; E. C. and Y. L. formal analysis; E. C., H. K., and D.-K. K. methodology; E. C. and Y. L. writing-original draft; E. C., H. K., D.-K. K., and Y. L. writing-review and editing; H. K. and D.-K. K. software; H. K. and D.-K. K. visualization; Y. L. supervision; Y. L. funding acquisition; Y. L. investigation; Y. L. project administration.

Acknowledgments—We thank Dr. Timothy A Hacker for performing echocardiography and Dr. Matthew Brody for valuable discussions and critical reading of the manuscript.

References

1. Ziaeian, B., and Fonarow, G. C. (2016) Epidemiology and aetiology of heart failure. *Nat. Rev. Cardiol.* **13,** 368–378 CrossRef Medline
2. McNally, E. M., Golbus, J. R., and Puckelwartz, M. J. (2013) Genetic mutations and mechanisms in dilated cardiomyopathy. *J. Clin. Invest.* **123,** 19–26 CrossRef Medline
3. Hall, D. D., Ponce, J. M., Chen, B., Spitler, K. M., Alexia, A., Oudit, G. Y., Song, L. S., and Grueter, C. E. (2017) Ectopic expression of Cdk8 induces eccentric hypertrophy and heart failure. *JCI Insight* **2,** 92476 Medline
4. van Berlo, J. H., Maillet, M., and Molkentin, J. D. (2013) Signaling effectors underlying pathologic growth and remodeling of the heart. *J. Clin. Invest.* **123,** 37–45 CrossRef Medline
5. Ujfalusi, Z., Vera, C. D., Mijailovich, S. M., Svicevic, M., Yu, E. C., Kawana, M., Ruppel, K. M., Spudich, J. A., Geeves, M. A., and Leinwand, L. A. (2018) Dilated cardiomyopathy myosin mutants have reduced force-generating capacity. *J. Biol. Chem.* **293,** 9017–9029 CrossRef Medline
6. Camacho, P., Fan, H., Liu, Z., and He, J. Q. (2016) Small mammalian animal models of heart disease. *Am. J. Cardiovasc. Dis.* **6,** 70–80 Medline
7. Bang, M. L. (2017) Animal models of congenital cardiomyopathies associated with mutations in Z-line proteins. *J. Cell. Physiol.* **232,** 38–52 CrossRef Medline
8. McNally, E. M., and Mestroni, L. (2017) Dilated cardiomyopathy: genetic determinants and mechanisms. *Circ. Res.* **121,** 731–748 CrossRef Medline
9. Brody, M. J., Hacker, T. A., Patel, J. R., Feng, L., Sadoshima, J., Tevosian, S. G., Balijepalli, R. C., Moss, R. L., and Lee, Y. (2012) Ablation of the cardiac-specific gene leucine-rich repeat containing 10 (Lrrc10) results in dilated cardiomyopathy. *PLoS One* **7,** e51621 CrossRef Medline
10. Taegtmeyer, H., Sen, S., and Vela, D. (2010) Return to the fetal gene program: a suggested metabolic link to gene expression in the heart. *Ann. N.Y. Acad. Sci.* **1188,** 191–198 CrossRef Medline
11. Naqvi, N., Li, M., Calvert, J. W., Tejada, T., Lambert, J. P., Wu, J., Kesteven, S. H., Holman, S. R., Matsuda, T., Lovelock, J. D., Howard, W. W., Iismaa, S. E., Chan, A. Y., Crawford, B. H., Wagner, M. B., *et al.* (2014) A proliferative burst during preadolescence establishes the final cardiomyocyte number. *Cell* **157,** 795–807 CrossRef Medline
12. Morton, S. U., and Brodsky, D. (2016) Fetal physiology and the transition to extrauterine life. *Clin. Perinatol.* **43,** 395–407 CrossRef Medline
13. Tzahor, E., and Poss, K. D. (2017) Cardiac regeneration strategies: staying young at heart. *Science* **356,** 1035–1039 CrossRef Medline
14. Harvey, R. P., Wystub-Lis, K., del Monte-Nieto, G., Graham, R. M., and Tzahor, E. (2016) Cardiac regeneration therapies: targeting neuregulin 1 signalling. *Heart Lung Circ.* **25,** 4–7 CrossRef Medline
15. D'Uva, G., Aharonov, A., Lauriola, M., Kain, D., Yahalom-Ronen, Y., Carvalho, S., Weisinger, K., Bassat, E., Rajchman, D., Yifa, O., Lysenko, M., Konfino, T., Hegesh, J., Brenner, O., Neeman, M., *et al.* (2015) ERBB2 triggers mammalian heart regeneration by promoting cardiomyocyte dedifferentiation and proliferation. *Nat. Cell Biol.* **17,** 627–638 CrossRef Medline
16. Mercurio, V., Pirozzi, F., Lazzarini, E., Marone, G., Rizzo, P., Agnetti, G., Tocchetti, C. G., Ghigo, A., and Ameri, P. (2016) Models of heart failure based on the cardiotoxicity of anticancer drugs. *J. Card. Fail.* **22,** 449–458 CrossRef Medline
17. Rupert, C. E., and Coulombe, K. L. (2015) The roles of neuregulin-1 in cardiac development, homeostasis, and disease. *Biomark Insights* **10,** 1–9
18. Lemmens, K., Doggen, K., and De Keulenaer, G. W. (2007) Role of neuregulin-1/ErbB signaling in cardiovascular physiology and disease: implications for therapy of heart failure. *Circulation* **116,** 954–960 CrossRef Medline
19. Jung, J., Mysliwiec, M. R., and Lee, Y. (2005) Roles of JUMONJI in mouse embryonic development. *Dev. Dyn.* **232,** 21–32 CrossRef Medline
20. Mysliwiec, M. R., Bresnick, E. H., and Lee, Y. (2011) Endothelial Jarid2/Jumonji is required for normal cardiac development and proper Notch1 expression. *J. Biol. Chem.* **286,** 17193–17204 CrossRef Medline
21. Cho, E., Mysliwiec, M. R., Carlson, C. D., Ansari, A., Schwartz, R. J., and Lee, Y. (2018) Cardiac-specific developmental and epigenetic functions of Jarid2 during embryonic development. *J. Biol. Chem.* **293,** 11659–11673 CrossRef Medline
22. Landeira, D., and Fisher, A. G. (2011) Inactive yet indispensable: the tale of Jarid2. *Trends Cell Biol.* **21,** 74–80 CrossRef Medline
23. Mysliwiec, M. R., Carlson, C. D., Tietjen, J., Hung, H., Ansari, A. Z., and Lee, Y. (2012) Jarid2 (Jumonji, AT rich interactive domain 2) regulates NOTCH1 expression via histone modification in the developing heart. *J. Biol. Chem.* **287,** 1235–1241 CrossRef Medline
24. Kim, T. G., Chen, J., Sadoshima, J., and Lee, Y. (2004) Jumonji represses atrial natriuretic factor gene expression by inhibiting transcriptional activities of cardiac transcription factors. *Mol. Cell. Biol.* **24,** 10151–10160 CrossRef Medline
25. Bovill, E., Westaby, S., Reji, S., Sayeed, R., Crisp, A., and Shaw, T. (2008) Induction by left ventricular overload and left ventricular failure of the human Jumonji gene (JARID2) encoding a protein that regulates tran-

scription and reexpression of a protective fetal program. *J. Thorac. Cardiovasc. Surg.* **136,** 709–716 CrossRef Medline
26. Seok, H. Y., Chen, J., Kataoka, M., Huang, Z. P., Ding, J., Yan, J., Hu, X., and Wang, D. Z. (2014) Loss of MicroRNA-155 protects the heart from pathological cardiac hypertrophy. *Circ. Res.* **114,** 1585–1595 CrossRef Medline
27. Lee, Y., Song, A. J., Baker, R., Micales, B., Conway, S. J., and Lyons, G. E. (2000) Jumonji, a nuclear protein that is necessary for normal heart development. *Circ. Res.* **86,** 932–938 CrossRef Medline
28. Moses, K. A., DeMayo, F., Braun, R. M., Reecy, J. L., and Schwartz, R. J. (2001) Embryonic expression of an Nkx2–5/Cre gene using ROSA26 reporter mice. *Genesis* **31,** 176–180 CrossRef Medline
29. Mysliwiec, M. R., Chen, J., Powers, P. A., Bartley, C. R., Schneider, M. D., and Lee, Y. (2006) Generation of a conditional null allele of jumonji. *Genesis* **44,** 407–411 CrossRef Medline
30. Costa-Silva, J., Domingues, D., and Lopes, F. M. (2017) RNA-Seq differential expression analysis: an extended review and a software tool. *PLoS One* **12,** e0190152 CrossRef Medline
31. Baker, A. H., and Péault, B. (2016) A Gli(1)ttering role for perivascular stem cells in blood vessel remodeling. *Cell Stem Cell* **19,** 563–565 CrossRef Medline
32. Kramann, R., Schneider, R. K., DiRocco, D. P., Machado, F., Fleig, S., Bondzie, P. A., Henderson, J. M., Ebert, B. L., and Humphreys, B. D. (2015) Perivascular Gli1+ progenitors are key contributors to injury-induced organ fibrosis. *Cell Stem Cell* **16,** 51–66 CrossRef Medline
33. Zhao, J., and Liem, R. K. (2016) α-Internexin and peripherin: expression, assembly, functions, and roles in disease. *Methods Enzymol.* **568,** 477–507 CrossRef Medline
34. Vogel, P., Hansen, G., Fontenot, G., and Read, R. (2010) Tubulin tyrosine ligase-like 1 deficiency results in chronic rhinosinusitis and abnormal development of spermatid flagella in mice. *Vet. Pathol.* **47,** 703–712 CrossRef Medline
35. Somekawa, S., Imagawa, K., Hayashi, H., Sakabe, M., Ioka, T., Sato, G. E., Inada, K., Iwamoto, T., Mori, T., Uemura, S., Nakagawa, O., and Saito, Y. (2012) Tmem100, an ALK1 receptor signaling-dependent gene essential for arterial endothelium differentiation and vascular morphogenesis. *Proc. Natl. Acad. Sci. U.S.A.* **109,** 12064–12069 CrossRef Medline
36. Mizuta, K., Sakabe, M., Hashimoto, A., Ioka, T., Sakai, C., Okumura, K., Hattammaru, M., Fujita, M., Araki, M., Somekawa, S., Saito, Y., and Nakagawa, O. (2015) Impairment of endothelial-mesenchymal transformation during atrioventricular cushion formation in Tmem100 null embryos. *Dev. Dyn.* **244,** 31–42 CrossRef Medline
37. Talukder, M. A., Kalyanasundaram, A., Zhao, X., Zuo, L., Bhupathy, P., Babu, G. J., Cardounel, A. J., Periasamy, M., and Zweier, J. L. (2007) Expression of SERCA isoform with faster Ca^{2+} transport properties improves postischemic cardiac function and Ca^{2+} handling and decreases myocardial infarction. *Am. J. Physiol. Heart Circ. Physiol.* **293,** H2418–H2428 CrossRef Medline
38. Rosenthal, F., Feijs, K. L., Frugier, E., Bonalli, M., Forst, A. H., Imhof, R., Winkler, H. C., Fischer, D., Caflisch, A., Hassa, P. O., Lüscher, B., and Hottiger, M. O. (2013) Macrodomain-containing proteins are new mono-ADP-ribosylhydrolases. *Nat. Struct. Mol. Biol.* **20,** 502–507 CrossRef Medline
39. Smith, S. J., Towers, N., Saldanha, J. W., Shang, C. A., Mahmood, S. R., Taylor, W. R., and Mohun, T. J. (2016) The cardiac-restricted protein ADP-ribosylhydrolase-like 1 is essential for heart chamber outgrowth and acts on muscle actin filament assembly. *Dev. Biol.* **416,** 373–388 CrossRef Medline
40. Zeqiraj, E., Tang, X., Hunter, R. W., García-Rocha, M., Judd, A., Deak, M., von Wilamowitz-Moellendorff, A., Kurinov, I., Guinovart, J. J., Tyers, M., Sakamoto, K., and Sicheri, F. (2014) Structural basis for the recruitment of glycogen synthase by glycogenin. *Proc. Natl. Acad. Sci. U.S.A.* **111,** E2831–E2840 CrossRef Medline
41. Laforêt, P., Malfatti, E., and Vissing, J. (2017) Update on new muscle glycogenosis. *Curr. Opin. Neurol.* **30,** 449–456 CrossRef Medline
42. Lubelwana Hafver, T., Wanichawan, P., Manfra, O., de Souza, G. A., Lunde, M., Martinsen, M., Louch, W. E., Sejersted, O. M., and Carlson, C. R. (2017) Mapping the *in vitro* interactome of cardiac sodium (Na^+)–calcium (Ca^{2+}) exchanger 1 (NCX1). *Proteomics* **17,** 201600417 CrossRef Medline
43. Fahrenbach, J. P., Stoller, D., Kim, G., Aggarwal, N., Yerokun, B., Earley, J. U., Hadhazy, M., Shi, N. Q., Makielski, J. C., and McNally, E. M. (2014) Abcc9 is required for the transition to oxidative metabolism in the newborn heart. *FASEB J.* **28,** 2804–2815 CrossRef Medline
44. Mohammed Abdul, K. S., Jovanović, S., Du, Q., Sukhodub, A., and Jovanović, A. (2015) A link between ATP and SUR2A: a novel mechanism explaining cardioprotection at high altitude. *Int. J. Cardiol.* **189,** 73–76 CrossRef Medline
45. Gorsi, B., Whelan, S., and Stringer, S. E. (2010) Dynamic expression patterns of 6-*O* endosulfatases during zebrafish development suggest a sub-functionalisation event for sulf2. *Dev. Dyn.* **239,** 3312–3323 CrossRef Medline
46. Dupays, L., Kotecha, S., Angst, B., and Mohun, T. J. (2009) Tbx2 misexpression impairs deployment of second heart field derived progenitor cells to the arterial pole of the embryonic heart. *Dev. Biol.* **333,** 121–131 CrossRef Medline
47. Qu, X., Jia, H., Garrity, D. M., Tompkins, K., Batts, L., Appel, B., Zhong, T. P., and Baldwin, H. S. (2008) Ndrg4 is required for normal myocyte proliferation during early cardiac development in zebrafish. *Dev. Biol.* **317,** 486–496 CrossRef Medline
48. Ling, S. S. M., Chen, Y. T., Wang, J., Richards, A. M., and Liew, O. W. (2017) Ankyrin repeat domain 1 protein: a functionally pleiotropic protein with cardiac biomarker potential. *Int. J. Mol. Sci.* **18,** E1362 Medline
49. Goldbergova, M. P., Parenica, J., Jarkovsky, J., Kala, P., Poloczek, M., Manousek, J., Kluz, K., Kubkova, L., Littnerova, S., Tesak, M., Toman, O., Pavek, N., Cermakova, Z., Tomandl, J., Vasku, A., *et al.* (2012) The association between levels of tissue inhibitor of metalloproteinase-1 with acute heart failure and left ventricular dysfunction in patients with ST elevation myocardial infarction treated by primary percutaneous coronary intervention. *Genet. Test. Mol. Biomarkers* **16,** 1172–1178 CrossRef Medline
50. Porayette, P., Fruitman, D., Lauzon, J. L., Le Goff, C., Cormier-Daire, V., Sanders, S. P., Pinto-Rojas, A., and Perez-Atayde, A. R. (2014) Novel mutations in geleophysic dysplasia type 1. *Pediatr. Dev. Pathol.* **17,** 209–216 CrossRef Medline
51. Elahi, M. M., and Matata, B. M. (2014) Gender differences in the expression of genes involved during cardiac development in offspring from dams on high fat diet. *Mol. Biol. Rep.* **41,** 7209–7216 CrossRef Medline
52. Wang, F., Hou, J., Han, B., Nie, Y., Cong, X., Hu, S., and Chen, X. (2012) Developmental changes in lysophospholipid receptor expression in rodent heart from near-term fetus to adult. *Mol. Biol. Rep.* **39,** 9075–9084 CrossRef Medline
53. Kumar, D., Mains, R. E., and Eipper, B. A. (2016) 60 years of POMC: from POMC and α-MSH to PAM, molecular oxygen, copper, and vitamin C. *J. Mol. Endocrinol.* **56,** T63–T76 CrossRef Medline
54. O'Donnell, P. J., Driscoll, W. J., Bäck, N., Muth, E., and Mueller, G. P. (2003) Peptidylglycine-α-amidating monooxygenase and pro-atrial natriuretic peptide constitute the major membrane-associated proteins of rat atrial secretory granules. *J. Mol. Cell. Cardiol.* **35,** 915–922 CrossRef Medline
55. Young, P., Nie, J., Wang, X., McGlade, C. J., Rich, M. M., and Feng, G. (2005) LNX1 is a perisynaptic Schwann cell specific E3 ubiquitin ligase that interacts with ErbB2. *Mol. Cell Neurosci.* **30,** 238–248 CrossRef Medline
56. Mao, X., Gu, X., and Lu, W. (2017) GSG1L regulates the strength of AMPA receptor-mediated synaptic transmission but not AMPA receptor kinetics in hippocampal dentate granule neurons. *J. Neurophysiol.* **117,** 28–35 CrossRef Medline
57. Maurer, S. F., Fromme, T., Grossman, L. I., Hüttemann, M., and Klingenspor, M. (2015) The brown and brite adipocyte marker Cox7a1 is not required for non-shivering thermogenesis in mice. *Sci. Rep.* **5,** 17704 Medline
58. Huang, D., Liu, B., Huang, K., and Huang, K. (2018) Enoyl coenzyme A hydratase 1 protects against high-fat-diet-induced hepatic steatosis and insulin resistance. *Biochem. Biophys. Res. Commun.* **499,** 403–409 CrossRef Medline
59. Yin, Z., Ren, J., and Guo, W. (2015) Sarcomeric protein isoform transitions in cardiac muscle: a journey to heart failure. *Biochim. Biophys. Acta* **1852,** 47–52 CrossRef Medline

60. Pérez-Serra, A., Toro, R., Sarquella-Brugada, G., de Gonzalo-Calvo, D., Cesar, S., Carro, E., Llorente-Cortes, V., Iglesias, A., Brugada, J., Brugada, R., and Campuzano, O. (2016) Genetic basis of dilated cardiomyopathy. *Int. J. Cardiol.* **224,** 461–472 CrossRef Medline
61. He, A., Ma, Q., Cao, J., von Gise, A., Zhou, P., Xie, H., Zhang, B., Hsing, M., Christodoulou, D. C., Cahan, P., Daley, G. Q., Kong, S. W., Orkin, S. H., Seidman, C. E., Seidman, J. G., *et al.* (2012) Polycomb repressive complex 2 regulates normal development of the mouse heart. *Circ. Res.* **110,** 406–415 CrossRef Medline
62. Louzao-Martinez, L., Vink, A., Harakalova, M., Asselbergs, F. W., Verhaar, M. C., and Cheng, C. (2016) Characteristic adaptations of the extracellular matrix in dilated cardiomyopathy. *Int. J. Cardiol.* **220,** 634–646 CrossRef Medline
63. Li, L., Zhao, Q., and Kong, W. (2018) Extracellular matrix remodeling and cardiac fibrosis. *Matrix Biol.* **68–69**, 490–506 CrossRef Medline
64. Ghosh, A. K., Murphy, S. B., Kishore, R., and Vaughan, D. E. (2013) Global gene expression profiling in PAI-1 knockout murine heart and kidney: molecular basis of cardiac-selective fibrosis. *PLoS One* **8,** e63825 CrossRef Medline
65. Major, J. L., Dewan, A., Salih, M., Leddy, J. J., and Tuana, B. S. (2017) E2F6 impairs glycolysis and activates BDH1 expression prior to dilated cardiomyopathy. *PLoS One* **12,** e0170066 CrossRef Medline
66. Burke, M. A., Chang, S., Wakimoto, H., Gorham, J. M., Conner, D. A., Christodoulou, D. C., Parfenov, M. G., DePalma, S. R., Eminaga, S., Konno, T., Seidman, J. G., and Seidman, C. E. (2016) Molecular profiling of dilated cardiomyopathy that progresses to heart failure. *JCI Insight* **1,** e86898 Medline
67. Bersell, K., Arab, S., Haring, B., and Kühn, B. (2009) Neuregulin1/ErbB4 signaling induces cardiomyocyte proliferation and repair of heart injury. *Cell* **138,** 257–270 CrossRef Medline
68. Song, Y., Xu, J., Li, Y., Jia, C., Ma, X., Zhang, L., Xie, X., Zhang, Y., Gao, X., Zhang, Y., and Zhu, D. (2012) Cardiac ankyrin repeat protein attenuates cardiac hypertrophy by inhibition of ERK1/2 and TGF-β signaling pathways. *PLoS One* **7,** e50436 CrossRef Medline
69. Chen, C., Shen, L., Cao, S., Li, X., Xuan, W., Zhang, J., Huang, X., Bin, J., Xu, D., Li, G., Kitakaze, M., and Liao, Y. (2014) Cytosolic CARP promotes angiotensin II- or pressure overload-induced cardiomyocyte hypertrophy through calcineurin accumulation. *PLoS One* **9,** e104040 CrossRef Medline
70. Zhong, L., Chiusa, M., Cadar, A. G., Lin, A., Samaras, S., Davidson, J. M., and Lim, C. C. (2015) Targeted inhibition of ANKRD1 disrupts sarcomeric ERK-GATA4 signal transduction and abrogates phenylephrine-induced cardiomyocyte hypertrophy. *Cardiovasc. Res.* **106,** 261–271 CrossRef Medline
71. Mende, U., Kagen, A., Cohen, A., Aramburu, J., Schoen, F. J., and Neer, E. J. (1998) Transient cardiac expression of constitutively active Gαq leads to hypertrophy and dilated cardiomyopathy by calcineurin-dependent and independent pathways. *Proc. Natl. Acad. Sci. U.S.A.* **95,** 13893–13898 CrossRef Medline
72. Hou, N., Wen, Y., Yuan, X., Xu, H., Wang, X., Li, F., and Ye, B. (2017) Activation of Yap1/Taz signaling in ischemic heart disease and dilated cardiomyopathy. *Exp. Mol. Pathol.* **103,** 267–275 CrossRef Medline
73. Brody, M. J., Cho, E., Mysliwiec, M. R., Kim, T. G., Carlson, C. D., Lee, K. H., and Lee, Y. (2013) Lrrc10 is a novel cardiac-specific target gene of Nkx2–5 and GATA4. *J. Mol. Cell. Cardiol.* **62,** 237–246 CrossRef Medline
74. Nevil, M., Bondra, E. R., Schulz, K. N., Kaplan, T., and Harrison, M. M. (2017) Stable binding of the conserved transcription factor grainy head to its target genes throughout *Drosophila melanogaster* development. *Genetics* **205,** 605–620 CrossRef Medline
75. Langmead, B., Trapnell, C., Pop, M., and Salzberg, S. L. (2009) Ultrafast and memory-efficient alignment of short DNA sequences to the human genome. *Genome Biol.* **10,** R25 CrossRef Medline
76. Li, B., and Dewey, C. N. (2011) RSEM: accurate transcript quantification from RNA-Seq data with or without a reference genome. *BMC Bioinformatics* **12,** 323 CrossRef Medline
77. Huang, D. W, Sherman, B. T., and Lempicki, R. A. (2009) Systematic and integrative analysis of large gene lists using DAVID bioinformatics resources. *Nat. Protoc.* **4,** 44–57 CrossRef Medline
78. Huang, D. W., Sherman, B. T., and Lempicki, R. A. (2009) Bioinformatics enrichment tools: paths toward the comprehensive functional analysis of large gene lists. *Nucleic Acids Res.* **37,** 1–13 CrossRef Medline
79. Hosack, D. A., Dennis, G., Jr., Sherman, B. T., Lane, H. C., and Lempicki, R. A. (2003) Identifying biological themes within lists of genes with EASE. *Genome Biol.* **4,** R70 CrossRef Medline